Supporting Information

Ultra-Fast, Chemical-Free, Mass Production of High Quality Exfoliated Graphene

Aminul Islam[$], Biswajyoti Mukherjee[$], Krishna Kant Pandey, Anup Kumar Keshri[*]

Plasma Spray Coating Laboratory, Metallurgical and Materials Engineering Indian Institute of Technology Patna-801106, India

$: Both Authors has contributed equally

Table of Contents

S1: Graphene synthesis at high temperature

S2: DC plasma spray set-up

(a) Inert gas shroud attachment
(b) Temperature and velocity In-flight graphite particle

S3: As-received graphite powder

S4: Selection of plasma process parameters

S5: Plasma spraying of graphite powder particle

S6: Stability of exfoliated graphite in deionized water

S7: Evaluation of sprayed graphite powder by X-ray diffraction technique

S8: Evaluation of sprayed graphite powder by Raman Spectroscopy

S9: SEM images of exfoliated graphene at optimized parameter

S10: Dynamic Light Scattering of exfoliated graphene

S11: Evidence of single layer graphene from several spots

S12: Evidence of bi-/tri- layer graphene

S13: AFM images of exfoliated graphene

S14: FTIR spectra of exfoliated graphene coating

S15: Elaboration on exfoliation mechanism

S16: Evidence of few-layer graphene

S17: Yield calculation for plasma sprayed exfoliated graphene

S18: Price calculation of exfoliated graphene

S19: Comparison of achieved results with literatures

S20: Reproducibility of exfoliated graphene

S21: Experimental details on proof-of-concept of exfoliated graphene

(a) Layer-wise Young's modulus of exfoliated graphene
(b) Tribological test on exfoliated graphene coated substrate
(c) Layer-wise electrical conductivity of exfoliated graphene
(d) Transmittance test on exfoliated graphene coated substrate
(e) Electrochemical test of exfoliated graphene

S1: Graphene synthesis at high temperature

Different protocols, broadly classified as: bottom-up and top-down approaches have been explored for synthesizing graphene.[1] The bottom-up approach uses carbon-rich molecules to assemble and grow graphene whereas the top down approach uses the abundant source, *i.e.*, graphite and breaks them into its smaller entity.[1]

In bottom-up synthesis, temperature remains one of the critical parameters in realizing growth of graphene. As an example, chemical vapor deposition (CVD) is a straight forward approach that works by assembling carbon rich molecules over a pre-determined substrate at a certain temperature.[2-10] The temperature of the substrate is a primary condition that defines the type of reactions that will occur.[11] While, the advantage of CVD or epitaxial growth is the superior quality of the resulting graphene, the complexity of the process, dependency on substrate quality, along with low yield and high cost makes it difficult of mass produce graphene.[12-15] Another approach uses pyrolysis of carbon-rich molecules into graphene sheets using gas phase atmospheric plasma.[16-30] It involves the impingement of a carbon-containing precursor, into an atmospheric pressure (RF, DC or MW) generated plasma. It is a rapid process where carbon rich precursors, mainly hydrocarbons are introduced to high temperature (>3000K) plasma where they decompose to smaller carbon entities, and assemble to form graphene sheet. It is a rapid process and the entire steps are completed within seconds. The major drawback is the poor quality of graphene and ultra-low yield.[16,17]

However, exfoliating graphite using top-down approach into its smaller entity has made it possible to realize the bulk production of graphene to cater ever increasing industrial demands. Generally, graphite is composed of millions of graphene sheets held together by weak van der Waals forces. Since, no chemical bonds existed between adjacent graphene layers, it became the conventional approach for researchers to extract the individual layers from graphite. While,

solvent or surfactant assisted sonication exfoliation of graphite is widely studied, this technique employs extra agents in the reduction step that frequently introduces selected heteroatoms.[33-35] Most of these solvent possess high boiling point and removal is often very tedious and involves multiple cleaning steps. On the other hand, thermal exfoliation of graphite is believed to be a cleaner approach to mass cleaner to mass produce graphene. This is because thermal exfoliation of graphite doesn't require any organic solvent media avoiding multi-step cleaning. Moreover, this means of exfoliation is rapid and completed within minutes making thermal exfoliation a fast process with potential to mass produce graphene. Hence, the exfoliation of expanded graphite and intercalated graphite compounds at high temperature has been studied to realise graphene synthesis.[36-50] This process involves rapid heating functionalized/expanded graphite. The functional groups decompose at high temperature and yields gas which build enough pressure, enough to overcome the van der Waals attraction causing exfoliation. In past this technique has produced graphene with upto 80% single layers and specific surface area (upto 700–1500m^2/g).[33] However, at the same time, graphene produced using this approach is highly defective including topological defects. Moreover, this technique introduces unwanted functionalization due to the nature involved with the exfoliation.[52-55] XPS reveals unwanted doping in thermally exfoliated graphene thus forming trade-off in quality.[56-57] A pictorial representation of the development of high temperature graphene synthesis (bottom-up and top down) and product representation with respect to 6 critical elements *i.e.*, (1) defect, (2) yield, (3) cost, (4) purity, (5) production rate and (6) layers is provided in Figure S1 for clear understanding.

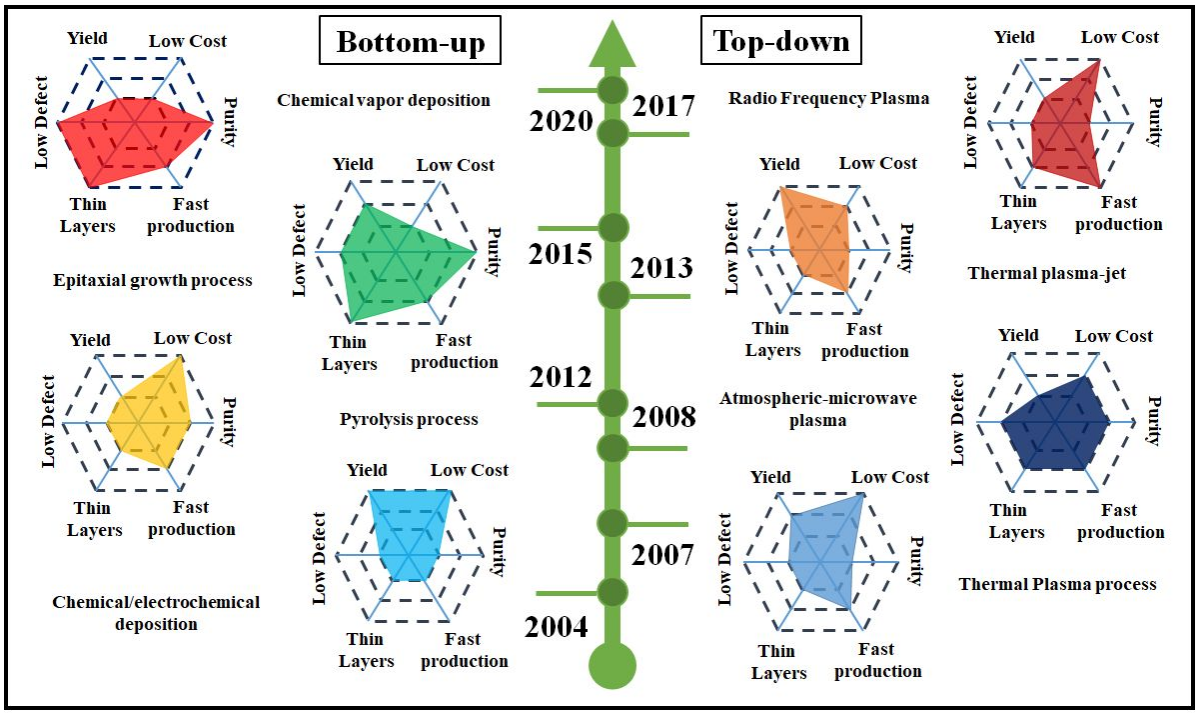

Figure S1: Timeline for development of high temperature graphene synthesis. Each product has been evaluated in terms of 6 critical elements: (1) defect, (2) yield, (3) cost, (4) purity, (5) production rate and (6) layers. The inner, middle and outer hexagon indicate low, medium and high levels, respectively. The statistics are based on literature data available in literature.

S2: DC plasma spray set-up

A DC atmospheric plasma spray system equipped with a DC torch (9MB, Oerlikon Metco, Switzerland) is used for exfoliating graphite. Argon and hydrogen (Purity 99.9%) were used as primary and secondary gasses respectively. All gasses were purchased from Praxair Inc., India, otherwise stated. Argon was also used as carrier gas, *i.e.*, to carry graphite powder through powder feeder (5MPE) to the plasma gun. The graphite is externally fed perpendicular to the plasma plume. An inert atmosphere shroud is fitted along with the plasma gun. The shroud delivers jet of argon gas along the plasma plume which provides insulation to the graphite particles from ambient atmosphere. An In-flight particle diagnostic sensor is placed at a

distance of 75 mm from the nozzle, perpendicular to the plasma plume for measuring temperature and velocity of sprayed graphite. More details about inert atmosphere shroud and in-flight diagnostic sensor is provided in independent section S2a and b. The DC plasma spray setup comprising of the gun, inert atmosphere shroud attachment, in-flight particle diagnostic sensor and powder collector chamber is shown in Figure S2.

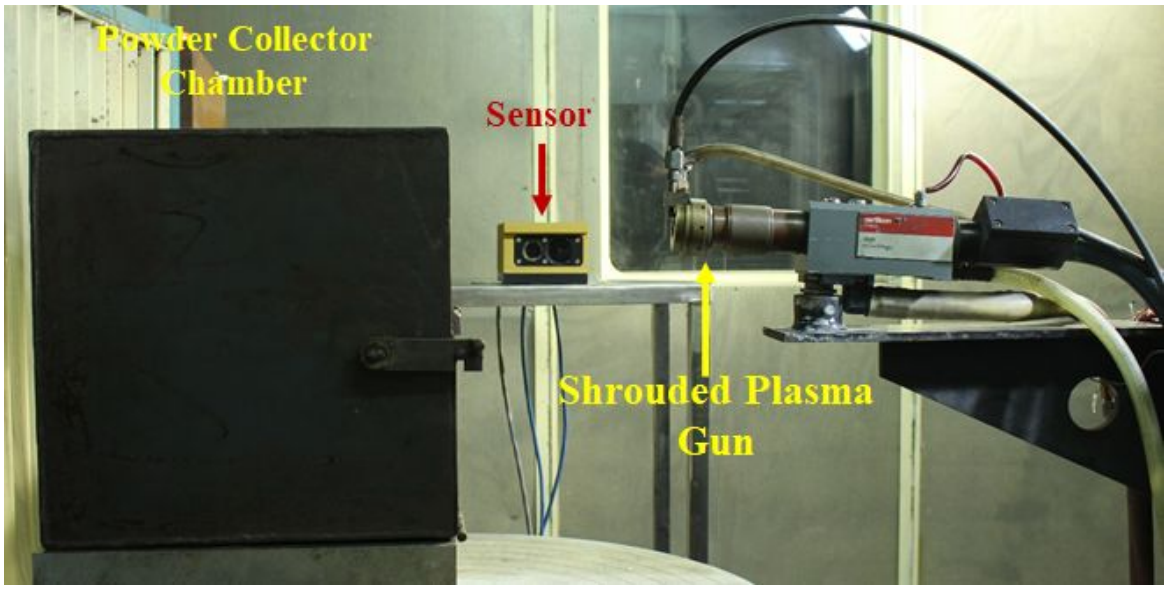

Figure S2: Digital image of the complete plasma spray setup for exfoliation of graphite

The complete plasma spray set-up is illustrated in Figure S2.1 as a schematic. The entire DC spray unit (shown Figure S2) is operated inside an Acoustic chamber. The acoustic chamber reduces the high noise levels during plasma spraying to an acceptable limit of 70 dBA. The chamber also contains dust collector that sucks the fly-away graphite particles, which otherwise could be potentially hazardous to the operator or anyone in the vicinity. A heat exchanger circulates cold de-ionized water to the plasma gun in-order to prevent it from overheating. The 9MC ensures accuracy and control of the plasma spray process. An automated single hopper 9MP powder feeder operating using gravimetric feed methodology provides powder to the plasma plume.

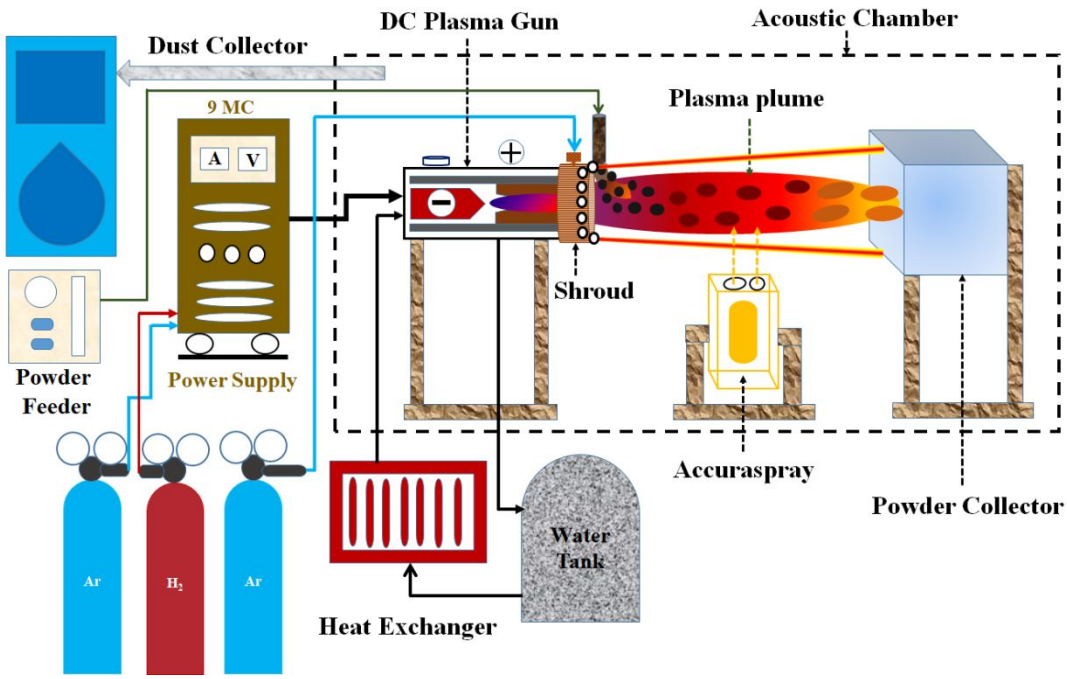

Figure S2.1: Schematic showing various components of plasma spray unit.

S2(a): Inert gas shroud attachment

The temperature involved in plasma spraying is very high (>10000 K at the core).[58] Hence, in ambient atmosphere, graphite powder exposed at this temperature will burn and decompose immediately. Therefore, preventing direct contact between the graphite powder and outside environment becomes necessary during plasma spraying. We therefore tried to cut down the contact between injected graphite powder at the plasma plume and outside environment using an inert atmosphere shroud (Figure S2.2a). The shroud is attached to the plasma gun/torch parallel to the nozzle exit (Figure S2.2b). The shroud shoots jet of inert gas through the perforated holes (represented by arrow in Figure S2.2a) that surrounds the plasma plume. This replicates an inert atmosphere, similar to the vacuum zone where the graphite powder and plasma plume come in contact. In past, the use of an inert shroud has proved to be effective in cutting down the powder-oxygen interaction.[59-60] Argon gas (Purity: 99.9%) is used as the inert shroud gas.

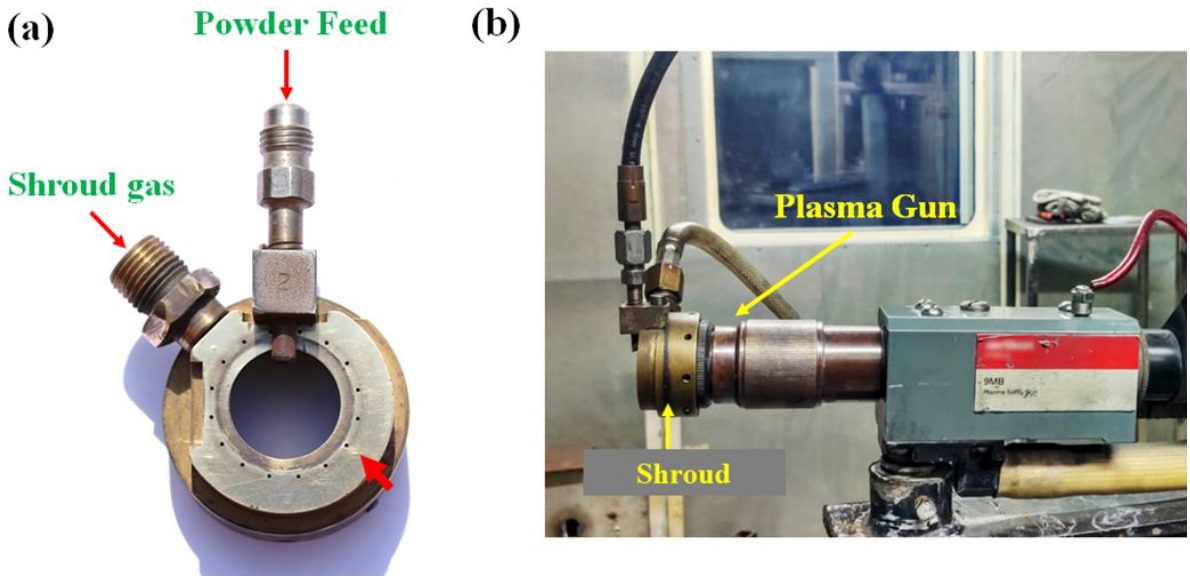

Figure S2.2:(a) Digital image of the shroud (b) the shroud attached to the plasma torch parallel to the nozzle exit.

S2(b): Temperature and velocity In-flight graphite particle

Temperature and velocity of the in-flight graphite is monitored using Accura Spray™ in-flight diagnostic sensor (Tecnar Automation, QC, Canada) (Figure S2.3a and b). This sensor provides average of temperature and velocities by collecting information in a measurement volume of ~75 mm^3.

The velocity of the in-flight particle is measured using the general 'time of flight' method. Two optical fibre senses the time travel of particle and the data is transmitted to a photomultiplier which generates electric pulse and calculate the travelling time and distance of the particle in-flight.

The temperature of the particle is measured by two colour pyrometry. Spectral energy of the in-flight particle in two different wavelength bands (785±20 and 995±20 nm) was

measured by two colour pyrometry and the surface temperature of the particle is acquired using Planck's law and Wein's approximation (below Eq.),[61]

$$\frac{1}{T} = \frac{\ln\left[\frac{\varepsilon_{(\lambda_1,T)}}{\varepsilon_{(\lambda_2,T)}}\left(\frac{\lambda_2}{\lambda_1}\right)^5 \frac{I_{(\lambda_2)}}{I_{(\lambda_1)}}\right]}{c_2\left(\frac{1}{\lambda_1} - \frac{1}{\lambda_2}\right)} \qquad [1$$

Where,λ_1 and λ_2 are the two wavelengths, and C_2 is constant (1.4388 cmK) while ε (λ,T) is the spectral emissivity. The lowest velocity and temperature that the sensor can measure is 5 m/s and 900°C respectively. The error in the measurement is less than 1.5 m/s for velocity and 15°C for temperature at a cross-correlation factor of 0.9.

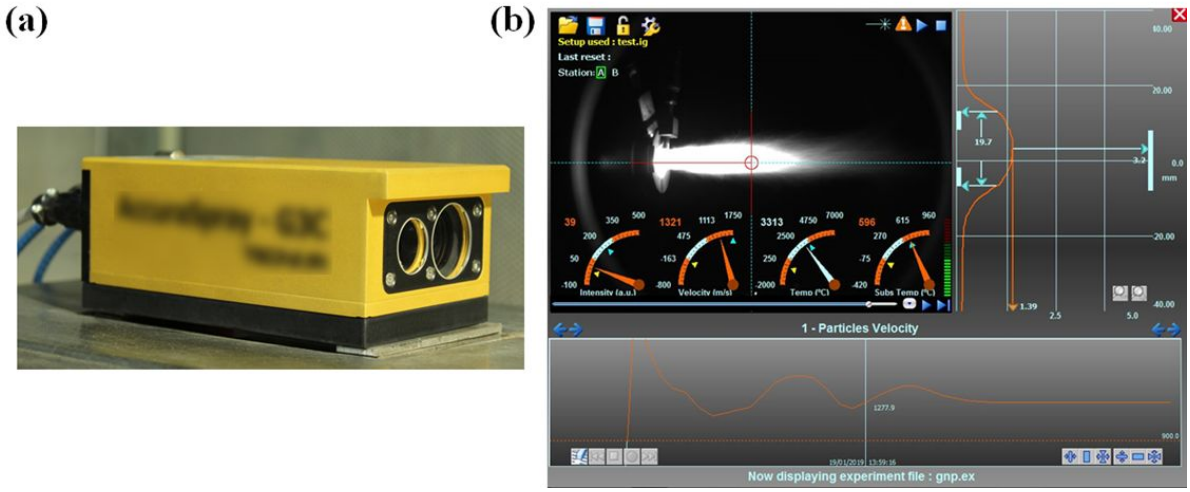

Figure S2.3: (a) Digital image of the In-flight particle diagnostic sensor; (b) screen showing live T and V of in-flight particle during the experiment.

S3: As-received graphite powder

Synthetic graphite powder was procured from Sigma-Aldrich (CAS Number 7782-42-5) (Figure S3a-b). Figure S3c shows Raman spectrum of the graphite. The spectrum shows peak at 1350 cm^{-1} (D-peak) corresponding to the breathing mode of sp^2 carbon atoms and 1582 cm^{-1} (G-peak). The D peak is associated with defects or disorders while the G peak is related to the in-phase vibrations of the graphite lattice. The 2D band with an overtone of the D-band indicates characteristics of stacked graphite.[62]

Scanning electron microscopy (SEM) shows that most of the particle size lies between 15-20 μm (lateral dimension) and are over 2 μm thick (Figure S3d-e). Figure S3f shows the N_2 adsorption isotherm of graphite obtained using a BET analyser (Autosorb iQ, Chemisorption, TCD, USA). The surface area of graphite was found to be 0.6 m^2/g, consistent with previous reports.[63] Figure S3g-h is the low magnification TEM image and characteristics SAED pattern of stacked graphite. High magnification TEM image of the graphite showing numerous graphitic lattice planes stacked one over another with lattice spacing 0.34 nm.

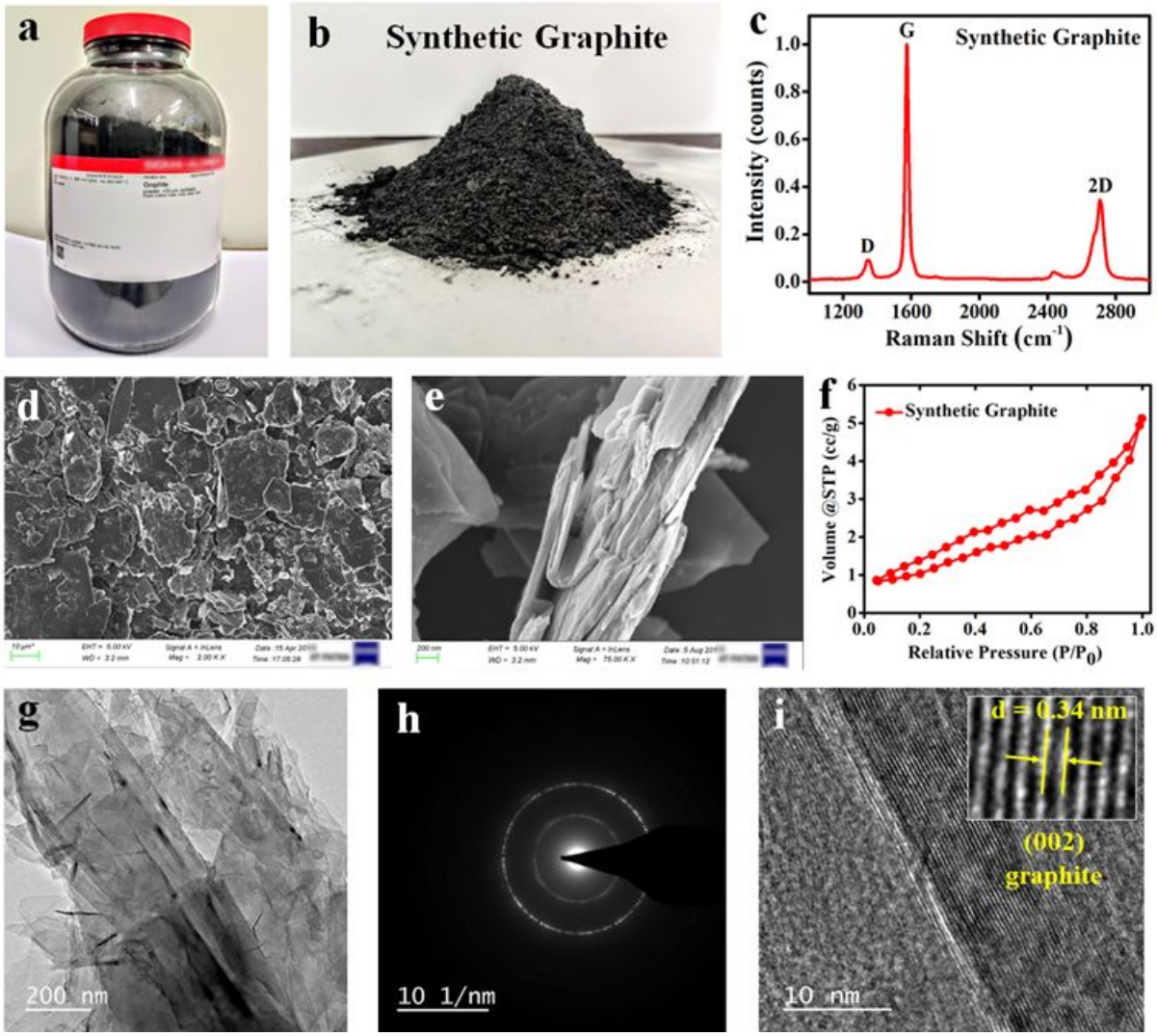

Figure S3: Image of (a-b) synthetic graphite powder(c) Raman Spectrum of graphite, SEM image of graphite flakes (d) top and (e) cross-sectional view, (f) BET isotherm of graphite, TEM image of graphite (g) low magnification image (h) SAED pattern and (i) high magnification image showing lattice plane of graphite.

S4: Selection of plasma process parameters

Our group has been studying the temperature (T) and velocity (V) profile and properties of in-flight sprayed particles.[64] Various parameters including plasma power, primary gas flow rate, powder feed rate, stand-off distance affect the T and V profile of any sprayed powder. Proper

control of T and V is necessary for successful exfoliation of graphite into graphene. However, powder feed rate and stand-off is of least concern in this study as these parameters play major role in controlling the thickness as well as tailoring the microstructure of the coating in any plasma spray coatings. Since, the aim of this work is to exfoliate graphite; not to deposit as film/coatings, we have eliminated powder feed rate and stand-off from our experiments. Out of these 4, plasma power and gas flow rate has the major impact in shaping the final T and V of the powder.[64] While feeding the graphite powder in plasma plume, the user has direct control over the selected parameters, *i.e.*, (1) plasma power (P), (2) primary gas flow rate (G).

In our previous study, we sprayed graphene nanoplatelets (GNP) at plasma power in a range of 10-18 kW and observed successful retention of graphitic structures as well as subsequent purification of the sprayed GNP.[59] Hence, the lower threshold of plasma power was chosen at 10 kW. To understand the role of parameters, upper limit of plasma power was set at 40 kW. We tried varying the plasma power more than 40 kW too. However, it was observed that light weight graphite particles were unable to penetrate into the plasma plume due to turbulent plume at higher power (> 40 kW). Additionally, as mentioned above our primary goal is to provide an industrial viable solution to produce graphene, higher plasma power could lead to wear of nozzle. Hence, operating at higher temperature may need the frequent replacement of nozzle, limiting its industrial potential. The lower and upper limit of primary gas flow rate was set between 80-140 SCFH. A total of 7 series of plasma power (P1=10, P2=15, P3=20, P4=25, P5=30, P6=35 and P7=40 kW) and 4 series of primary gas flow rate (G1=80, G2=100, G3=120 and G4=140 SCFH) were varied to obtain 28 experimental parameters. The graphite was fed at a constant rate (120 g/h). We used a nomenclature to identify the parameters set, for example parameters set P2G3 refer to Power 15 kW, and primary gas flow rate of 120 SCFH at feed rate 120 g/h.

S5: Plasma spraying of graphite powder

Plasma spraying of graphite powder was carried out at all the 28 numbers of different process parameters and the spraying was performed in an inert gas atmosphere. During the spraying, T and V of the particle was continuously monitored using the in-flight particle diagnostic sensor for every set of experiments, which has been tabulated in Table S5.

Table S5: Thermal and Kinetic history of in-flight graphite powder particle during the spraying process.

			Plasma Power (kW)						
			10 (P1)	**15 (P2)**	**20 (P3)**	**25 (P4)**	**30 (P5)**	**35 (P6)**	**40 (P7)**
Primary Gas Flow Rate (SCFH)	**80 (G1)**	**T (°C)**	2500±50	2900±45	3200±55	3400±45	3550±50	3650±52	3700 ± 53
		V (m/s)	205 ± 5.0	218 ± 4.0	232 ± 4.5	248 ± 5.5	263 ± 6.0	280 ± 5.0	295 ± 5.2
	100 (G2)	**T (°C)**	2350±50	2700±45	3000 ±55	3220 ±45	3400 ±50	3500 ±52	3550 ±53
		V (m/s)	230 ± 4.5	245 ± 3.9	262 ± 5.0	280 ± 4.5	295 ± 4.3	310 ± 4.0	322 ± 3.9
	120 (G3)	**T (°C)**	2220 ±42	2580 ±40	2870 ±43	3100 ±45	3280 ±45	3390 ±37	3430 ±42
		V (m/s)	260 ± 5.0	277 ± 4.8	292 ± 4.7	308 ± 4.0	323 ± 3.8	338 ± 4.5	350 ± 4.2
	140 (G4)	**T (°C)**	2100 ±50	2450 ±45	2750 ±55	2970 ±45	3150 ±50	3250 ±52	3300 ± 53
		V (m/s)	305 ± 5.0	322 ± 5.0	335 ± 5.0	348 ± 5.0	363 ± 4.5	377 ± 4.5	390 ± 4.5

S6: Stability of exfoliated graphite in deionized water

The plasma sprayed graphite powder was dispersed in deionized (DI) water and centrifuged at 1000 rpm for 1h to remove unexfoliated large agglomerates. The unexfoliated graphite settle down at the bottom while the lighter exfoliated graphene remains suspended as supernatant and can be separated. However, untreated graphene has the tendency to reaggregate and settle very quickly in DI water. Therefore, we collected the exfoliated graphene containing supernatant immediately (less than 5 min) after centrifuge. We believe that the exfoliated graphene does

not aggregate within themselves and settles within this time. In order to see the aggregation issue of our exfoliated graphene, we compared the absorbance of the supernatant (obtained after centrifuge) with respect to the time to observe the stability of graphene in DI water. We observed the stability of dispersion of the exfoliated graphene using an Ultraviolet–Visible spectrophotometer (Shimadzu, UV-2600, Japan). Absorbance at 650 nm is normally used to compare the stability of graphene in a dispersion study.[65] Figure S5 shows that the suspended exfoliated graphene doesn't settle even after 1h. Hence, the exfoliated graphene can be collected smoothly by removing the supernatant.

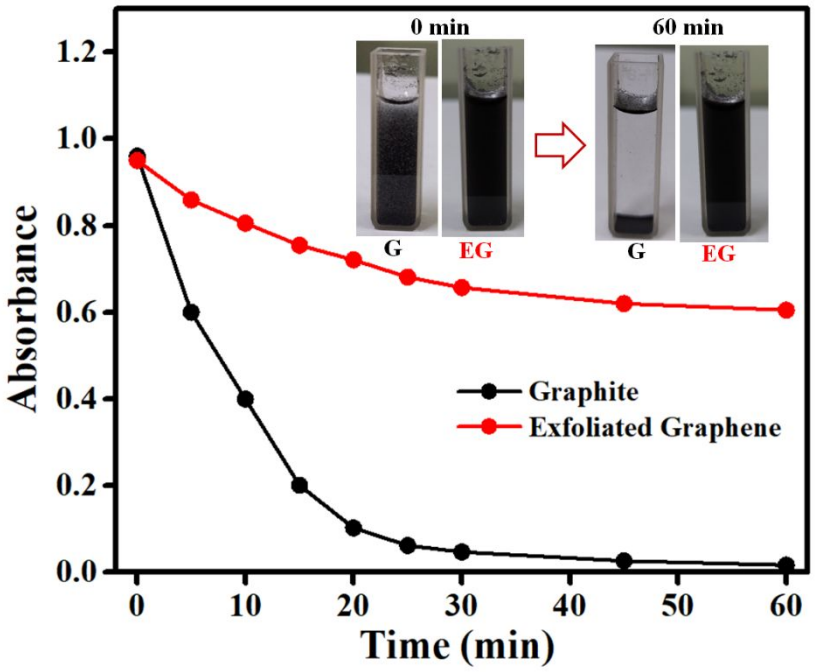

Figure S6: Stability of the supernatant in deionized water.

S7: Evaluation of sprayed graphite powder by X-ray diffraction technique

To get an insight on the exfoliation efficacy, all 28 samples of sprayed graphite were studied using X-Ray Diffractometer (Rigaku-X'Pert PRO, PANalytical, Japan). Intensity of the peak were recorded between diffraction angle 2θ= 23° to 30°using Cu/K_α (λ = 1.5418 Å) operating at 60 kV. Reduction in intensity of (002) plane is observed in all sprayed graphite (Figure S7),

which indicates the exfoliation of graphite layers.[66] The intensity values of all 28 samples for each process parameters have been shown in Figure S7 and the results has also been tabulated in Table S7. Based on the lowest peak intensity value of the samples, the level of exfoliation has been evaluated. Five (5) best parameters have been chosen for Raman spectroscopy analysis (next section S8), which showed the lower intensity among all.

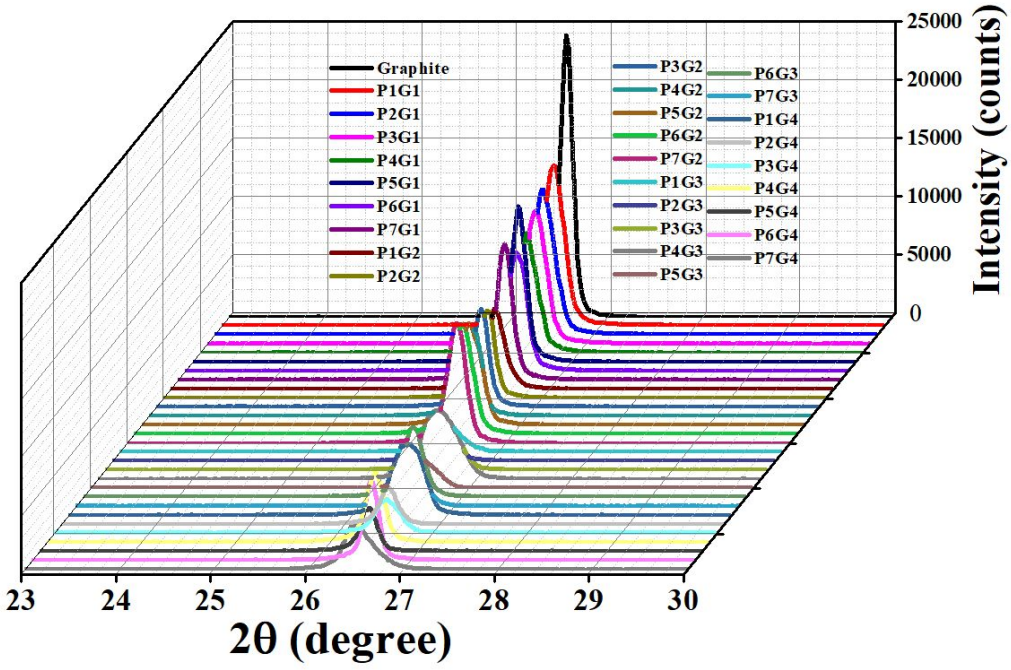

Figure S7: XRD spectra of plasma sprayed graphene. No normalization was done to distinguish the level of exfoliation in each samples.

Table S7: Peak intensity of sprayed graphite

SL. No.	Nomenclature	Processing Parameters		XRD information
		Power (kW)	Gas Flow (SCFH)	Intensity (002)
1	As received Graphite powder	--	--	25000
2	P1G1	10	80	13800

3	P1G2	10	100	6850
4	P1G3	10	120	2400
5	P1G4	10	140	6000
5	P2G1	15	80	12400
6	P2G2	15	100	7500
7	P2G3	15	120	2300
8	P2G4	15	140	3200
9	P3G1	20	80	11200
10	P3G2	20	100	8500
11	P3G3	20	120	3400
12	P3G4	20	140	2800
13	P4G1	25	80	10100
14	P4G2	25	100	7500
15	P4G3	25	120	5900
16	P4G4	25	140	6000
17	P5G1	30	80	13300
18	P5G2	30	100	8800
19	P5G3	30	120	2500
20	P5G4	30	140	3700
21	P6G1	35	80	9900
22	P6G2	35	100	9500
23	P6G3	35	120	6100
24	P6G4	35	140	6800
25	P7G1	40	80	11500

26	P7G2	40	100	10200
27	P7G3	40	120	2100
28	P7G4	40	140	3800

S8: Evaluation of sprayed graphite powder by Raman Spectroscopy

Samples from the 5 selected parameters were studied using Raman Spectroscopy (WiTec, CRM-2000, Germany). Raman spectra were gathered using an excitation laser wavelength of 514 nm and 50 mW power. For each samples, 15-20 spectra were collected. In past, Raman spectroscopy has been used extensively in determining the number of layers in graphene.[67-68] It holds good when the layers of graphene is less than 5-7. The full width at half-maximum (FWHM) of the 2D band has been used as a quantitative guide in determining number of layers in graphene. The Raman spectra will be analysed for the 2D band characteristics before selecting the best exfoliation parameter.

All samples displayed 2D band characteristics representative of few-layer graphene (Figure S8a-b). D-band was witnessed in each case with mean I_D/I_G ratios ranging between 0.17 and 0.23. Compared to pure graphite, the plasma spray exfoliated graphene showed high D peak (Figure S8b). This could be due to the irregular chirality along the edges of the exfoliated graphite.[69] Figure S8c is the plot of $I_D/I_{D'}$ for the 5 samples with values lower than sp^3 defect, basal plane defect and also edge defect level. It clearly indicates that the emergence of I_D peak might be due to the minor defects along the edge of exfoliated graphene.[70]

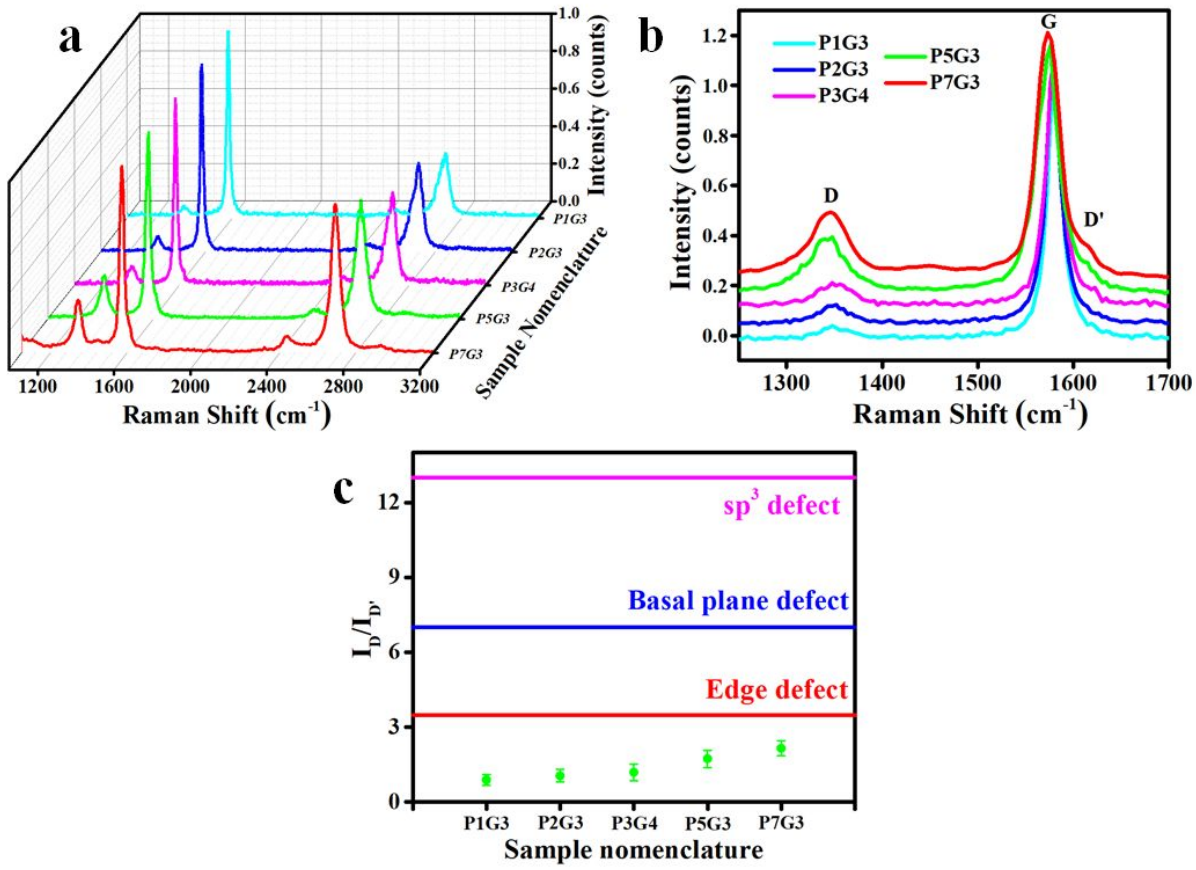

Figure S8:(a) Raman Spectra of 5 selected samples, (b) magnified Raman spectra showing D, G and D' peak for 5 selected samples and (c) Plot of $I_D/I_{D'}$ for 5 selected samples showing values less than 3.2 indicating no sp^3 and basal plane defect.

For investigating an individual graphene flake, the Raman mapping and spectra (at the basal plane and edge) was taken *in-situ* using an AFM integrated Raman Microscope (Alpha 300RA, WiTec, Germany). Excitation wavelength at 532 nm was obtained using Argon source. A laser beam size of ~ 1 μm with ×100 objective lens was used for measurements.

S9: SEM images of exfoliated graphene at optimized parameter

The sprayed graphite at parameter P7G3 was chosen based on best exfoliation efficacy. The exfoliated graphene was dispersed in ethanol and drop casted over a holey carbon grid. Images were captured using a FE-SEM (Carl Zeiss, Sigma-500, USA). Multiple batches were analysed to confirm the exfoliation efficacy, of which few images are presented here. Although SEM doesn't confirm the number of layers in the graphene, the transparent nature of the flakes (Figure S9a-i) definitely indicates reduction of layers compared to graphite (S3d-e).

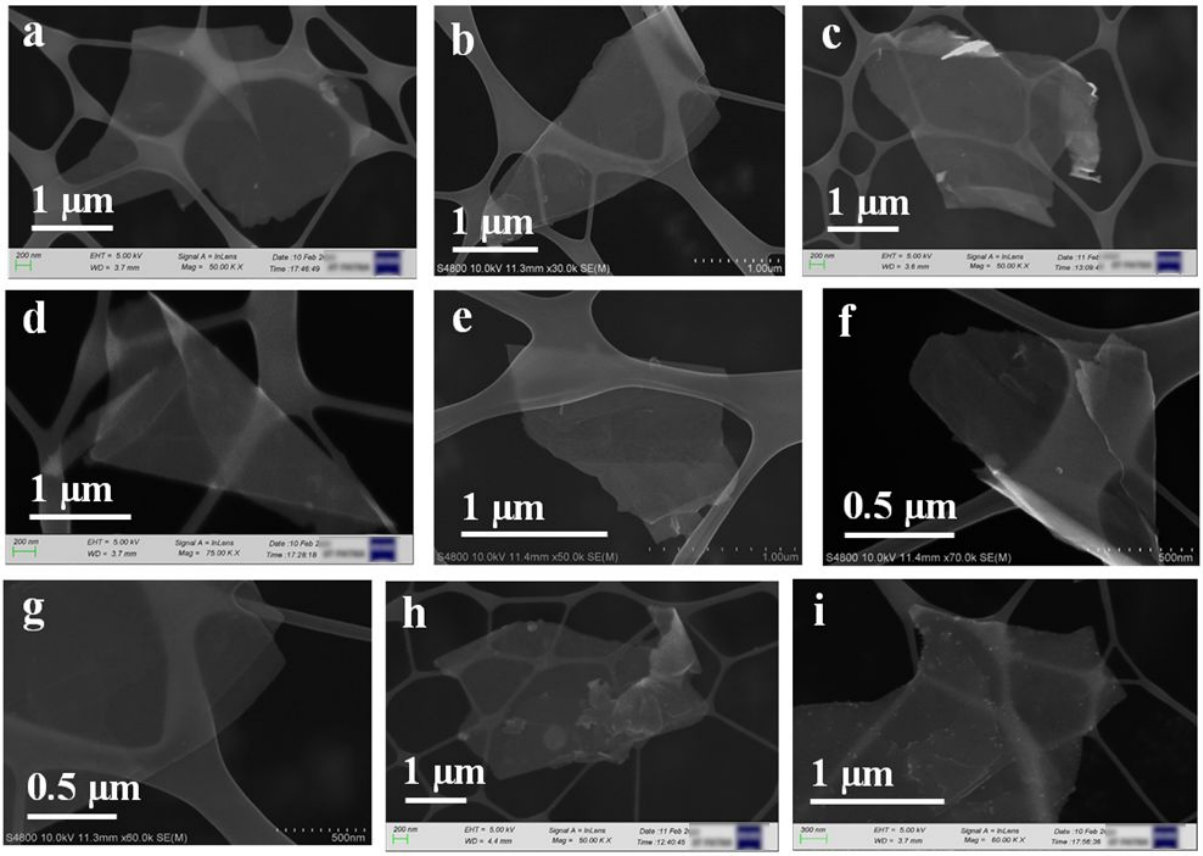

Figure S9: (a-i) shows the high magnification SEM images of exfoliated graphene. The transparent nature of the flakes indicates exfoliation of graphite to graphene. Also most of the flake length lies between 1-3 µm.

S10: Dynamic Light Scattering of the exfoliated graphene

The hydrodynamic diameter of the exfoliated graphene was measured using a dynamic light scattering analyser (Delsa™ Nano particle analyser, Beckman Coulter, USA). A total of 5 accumulation numbers with 25s duration were used for data acquisition.

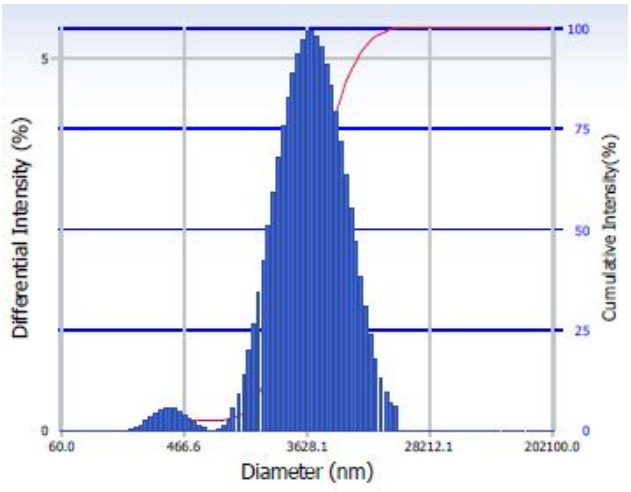

Figure S9: Size distribution curve obtained from dynamic light scattering measurement.

S11: Evidence of single layer graphene from several spots

For sample preparation, the exfoliated graphene was first sonicated in ethanol to remove agglomerates. The sonicated graphene was then drop-casted over TEM grid supported by holey carbon. The images were captured using a HR-TEM (JEM 2100F, JEOL-200, USA) with accelerating potential: 200 kV. Figure S11 shows the higher magnification TEM of some graphene flakes. Images captured from the edges of the graphene shows a bright edge without noticeable dark line along the edges depicting single layer. Figure S11d-f shows the normal-incidence electron diffraction pattern of the flake in Figure S11a-c. This pattern shows the typical six-fold symmetry. The ratio of intensity for I{1100}/I{2110} is greater than 1, indicative of single layer graphene.[67]

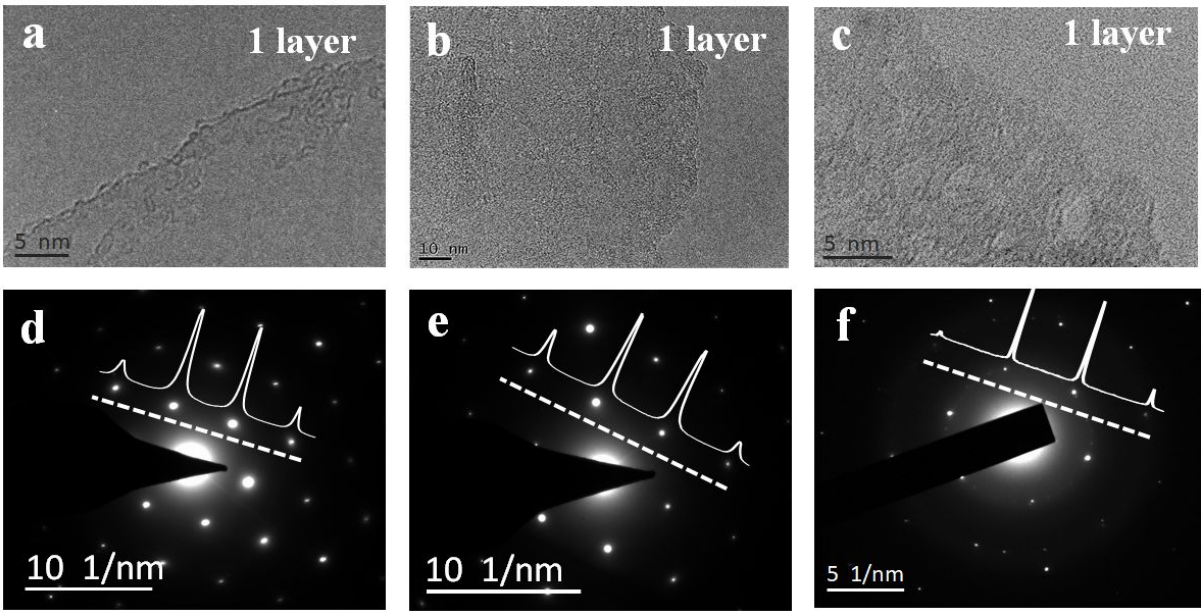

Figure S11: Evidence of single-layer graphene: (a-c) shows higher magnification HR-TEM images of exfoliated graphene and (d-f) corresponding SAED pattern of exfoliated graphene.

S12: Evidence of bi-/tri- layer graphene

Figure S12a-f shows higher magnification TEM images of some graphene flakes. The high magnification HR-TEM image on the edges of graphene showing 2 dark lines (in figure S12a-c) is indicative of bi-layer graphene, while 3 dark line (in figure S12d-f) is indicative of tri-layer graphene. The intensity ratio of the I{1100}/I{2110} is lesser than 1 as shown in Figure S12g-i, which is indicative of bi-/tri-layer graphene.[71]

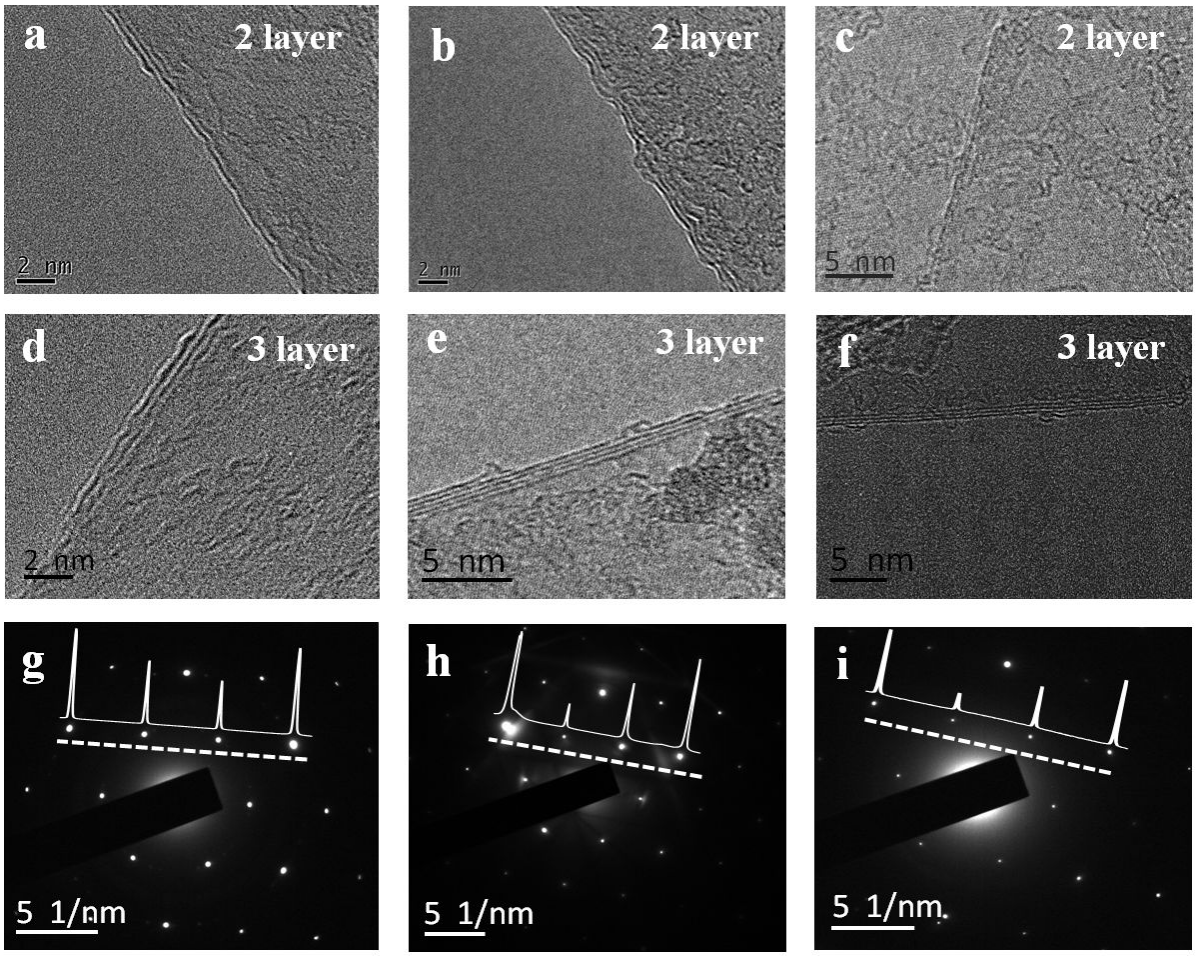

Figure S12: Evidence of bi-/tri-layer graphene. (a-c) shows higher magnification HR-TEM images of bi-layer graphene, (d-f) tri-layer graphene and (g-i) corresponding SAED pattern of exfoliated graphene flakes.

S13: AFM images of exfoliated graphene

The graphene flake images were acquired using a tapping mode Atomic Force Microscope (Asylum Research MFP-3D, USA). The exfoliated graphene was first dispersed in ethanol and spin-coated over a clean Si wafer. Multiple batches of samples were analysed and few images are presented here.

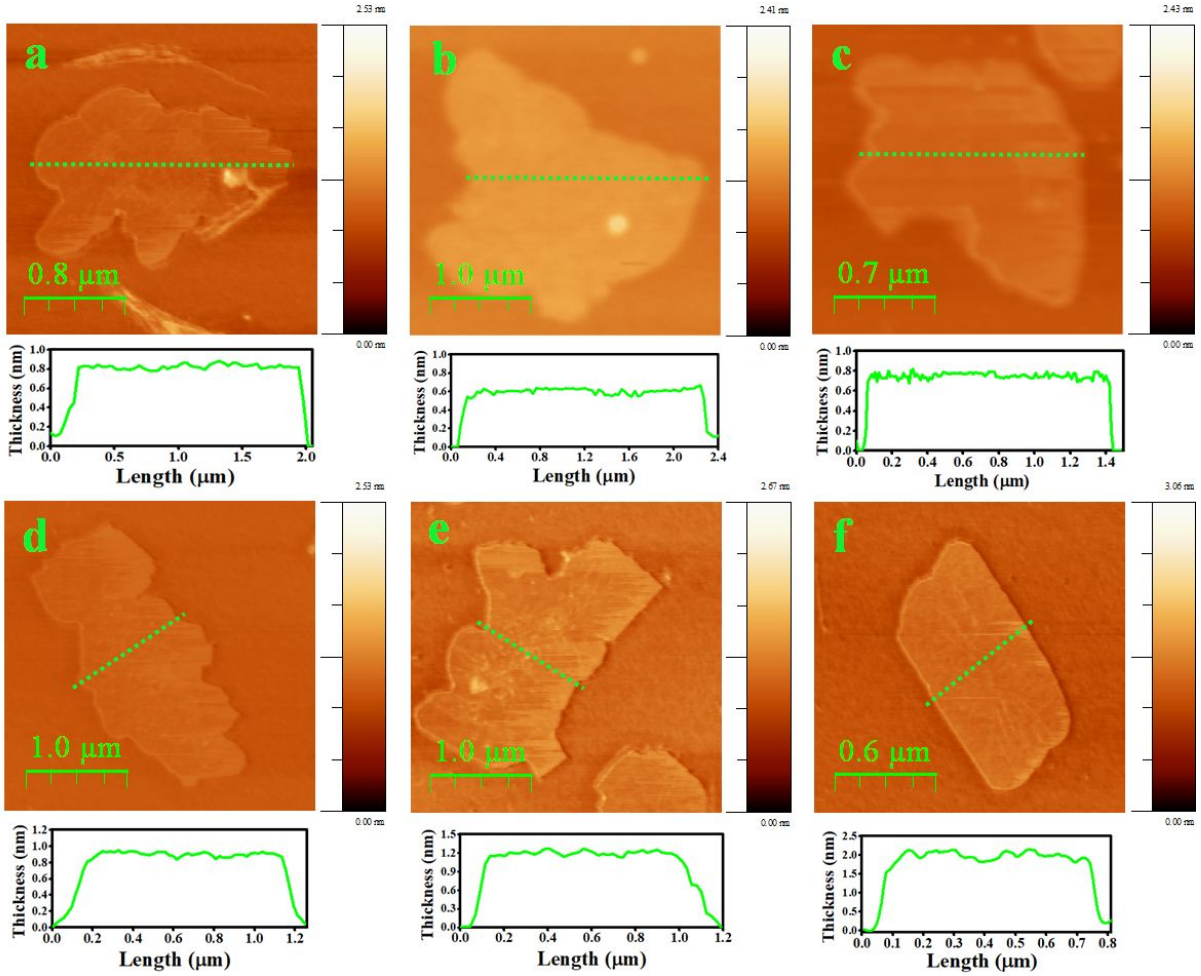

Fig S13: Tapping-mode AFM images of exfoliated graphene sheets.

S14: FTIR spectra of exfoliated graphene coating

One milligram of exfoliated graphene powder was mixed with 50 ml of ethanol by sonication. Further, mixed solution was coated over quartz substrate using spin coating technique. FTIR measurements were carried out using Nicolet iS10 spectrometer (Thermo Fisher Scientific, USA) in transmittance mode at room temperature. The spectrum was collected in the range of 1000-3000 cm^{-1}. The transmittance was evaluated over two samples *i.e.*, as prepared and air-dried graphene coated quartz as shown in Figure S14. The FTIR spectra depict nearly featureless spectra indicating that we produced pure graphene rather than some form of derivatised functionalized graphene.[67]

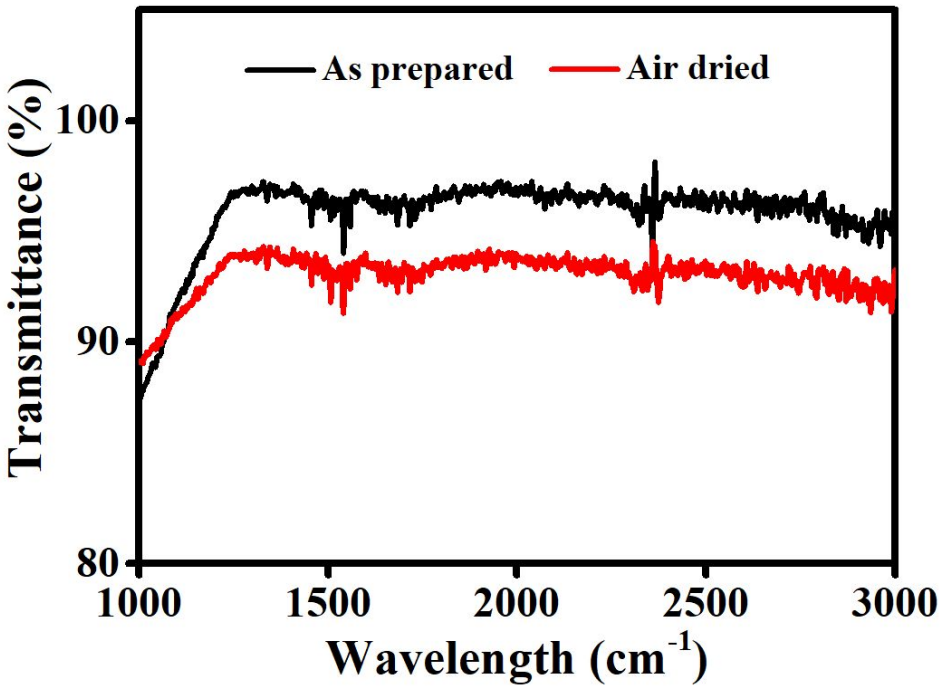

Figure S14: FTIR spectra of graphene coated quartz substrate (i) as prepared (black) and (ii) air dried (red) sample

S15: Elaboration on exfoliation mechanism

At the entry point of particle, the plume presents an abrupt laminar shear at the outer periphery of the jet and a few millimeters away from the nozzle, this laminar plasma plume breaks into large scale eddies and a fully turbulent zone is formed (as shown in the Figure 4c in main manuscript).[72-73] Upto the non-swirling (or Laminar region) condition of the plume, plasma arc is assumed symmetric and the two-dimensional Basset-Boussinesq-Ossen model equations are presented here to obtain the particle motion.[74]

$$\frac{dU_p}{dt} = -\frac{3\,\rho\,C_D}{4\rho_p D_P}(U_P - U)U_R + \sum F_R \qquad [2]$$

Where, subscript p denotes the particle, U represents the axial velocity component of plasma plume and ρ, C_D, D_p and F_R represents the density, drag coefficient, particle diameter and forces

affecting the particle motion trajectories, respectively.[75] Considering V as the radial velocity of plasma plume, the relative velocity of the particle in the plasma jet can be expressed as

$$U_R = \sqrt{(U - U_P)^2 + (V - V_P)^2} \quad [3]$$

The equation-2 has two components *i.e*. Drag force and the all the other forces (F_R) affecting the particle motion trajectories. The first term on the right hand side of equation 2 gives us the net drag force acting on the particles confined in the plasma jet. In the free flowing plasma jet, the drag force acting on the plume-particle system nullifies the effect of other minorly acting forces (F_R) such as gravity or buoyant force. Hence, upon increasing the velocity of the in-flight graphite particle by increasing the plasma gas flow rate, the drag force acting on the thermally shocked and weakened graphite particles also increase. However, at the same time, several reports have stated that the viscosity of argon may increase by nearly 8 folds in the high temperature of plume,[76] as compared to that at room temperature, which may decelerate the forward moving weakened graphite particle. Due to this, graphite particle will experience a shear force, which may lead to the initial exfoliation of graphite particle.

These weakened sheets further transcend towards downstream (*i.e*. turbulent region), where the main exfoliation takes place, assisted by shear between the layers. The external supply of argon gas (by shroud) throughout the periphery of the plume further reduces the enthalpy or temperature of the plasma, adding a more value to the quenching rate of the graphite during the whole process. A few millimetres away from the nozzle, the laminar plasma plume breaks into large scale eddies and a fully turbulent zone is formed.[77-80] This shroud argon additionally introduces an intense swirl around the whole circumference of the plasma, seeding a boost in the shear flow across the flow region and causes turbulence generation. The graphitic layers entrapped in this very region experience an intense lateral force on the upper lifted off graphite layers, as a cumulative effect of high flow rate of plasma gas and the external shroud gas.

Beyond a threshold value, this lateral force induces enough shear between the top layers and adjacent layers, causing their slippage over each other. The slippage between the layers lead to the exfoliation of the graphite into the plasma plume during whole continuous plasma spray process.

S16: Evidence of few-layer graphene

We have already seen the exfoliation of graphite to monolayer with exception of bi and tri layer in the powder sprayed at P7G3 process parameter (plasma power: 40 kW and primary gas flow rate of 120 SCHF). Temperature and velocity of the powder was recorded as 3430ºC and 350 m/s respectively at the P7G3 parameters. To confirm our understanding about the role of temperature and velocity on the exfoliation, we further analysed the exfoliated graphene sprayed at P5G3 process parameters (plasma power: 30 kW and primary gas flow rate of 120 SCHF) using TEM. Temperature and velocity of the powder was recorded as 3280ºC and 323 m/s respectively at the P5G3 parameters.) Figure S16a-c shows low magnification HR-TEM images of exfoliated graphene and S16d-f illustrate the evidence of few layer graphene. Figure S16g-i is the normal-incidence selected-area diffraction (SEAD) patterns demonstrating few layer graphene. TEM analysis of the exfoliated graphene showed the presence of few layer graphene and we have not observed the presence of monolayer graphene. This definitely confirms that right combination of temperature and velocity has strong impact on the layer of graphene. With the more rigorous trial, plasma process parameter can be optimized to achieve the exact number of graphene layer.

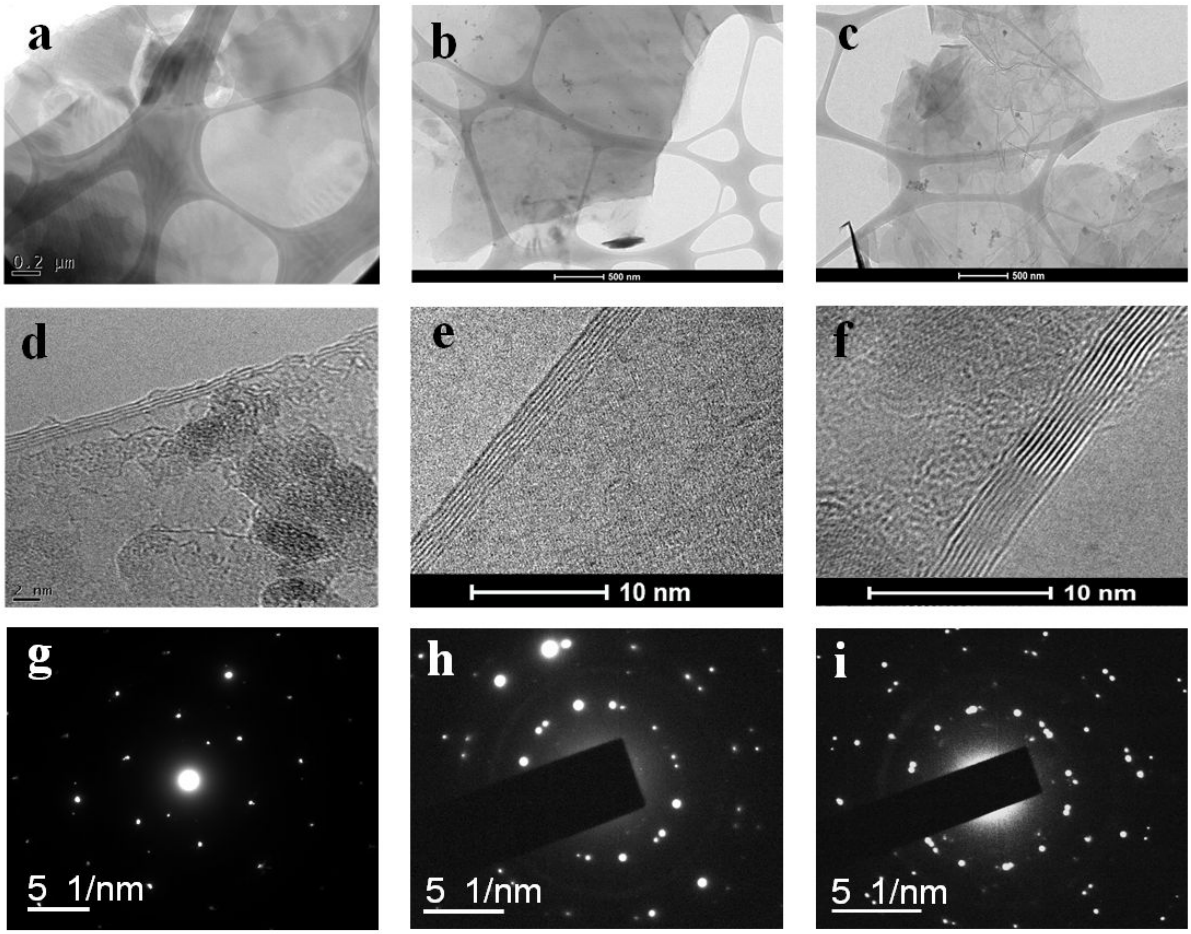

Figure **S16**: (a-c) shows low magnification HR-TEM images of exfoliated graphene, (d-f) shows evidence of few layer graphene and (g-i) Normal-incidence selected-area diffraction patterns (SEAD) pattern demonstrating few layer graphene. Rather than having only 6 spots in each ring of the pattern as in the case for single and AB-stacked multi-layer graphene, several orders of 6 spots (6, 12, 18 *etc*.) appear for misoriented layers also appears (Figure S14 h,i). This is due to the overlap of graphene sheets at misaligned angle and is known as Turbostratic Graphene.[81-82]

S17: Yield calculation for plasma sprayed exfoliated graphene

For the mass production of graphene, yield approach needs to be improved. While, the bottom-up production methods can produce pristine single to few layer graphene over a large area, it lacks massive scale-up opportunities. On the other hand, exfoliation of graphite to graphite

though proved to scale up graphene production suffers from low yield and incomplete exfoliation.[33,83] Recently, attempts were made and improvements were achieved in increasing yield of graphene using top down approaches. However, most of them lacked standardization which led to overestimation of yield. For example, most top down approaches calculate yield by dividing the product liberated by the total graphene used. Hence, we have determined our yield as the product obtained after plasma exfoliation and mild centrifugation, with no extra separation steps that reduce the yield.

For calculating our yield, we prepared a total of five batches of graphene. Feed rate of graphite was maintained at 120 g/h for the entire set of batches. The plasma sprayed graphite was collected in a chamber. The collected powder was centrifuged at mild rpm (~1000 rpm) for 1 hour in deionized water. Before centrifugation, the powder was well mixed in deionized water by shaker for 15 min. After centrifuge, the supernatant was separated from the heavy particles settled at bottom. The final powder was collected and heated overnight at 200°C in hot air oven. The dried powder was measured using weighing balance and the yield was calculated with respect to initially feed powder. The yields for different batches are listed in Table S16. Our method results in yields of upto 40% of 1-3layer graphene with a production rate of upto 48 g/h.

Table S17: Yield calculation for exfoliated graphene

Batch	Feed rate (graphite)/min	Powder obtained (in g/10 min)	Yield (%)	Production rate (g/h)
1	2	8.1	40.5%	48.2
2	2	7.1	35.2%	42.3
3	2	8.0	40.0%	48.1
4	2	7.9	39.8%	47.8
5	2	7.7	38.8%	46.6

Note that this yield can further be increased if the un-exfoliated graphite is recycled again. In order to demonstrate that the unexfoliated graphite can be recycled, we collected and dried it before spraying. The graphite is un-exfoliated or partially exfoliated graphite (Figure S17a). The powder was then plasma sprayed at similar parameter (Plasma power (P): 40 kW, gas flow rate (G): 120 SCFH). The sprayed powder was collected and centrifuged at 1000 rpm. The supernatant after centrifugation was analyzed using TEM, Raman spectroscopy and AFM. SAED displays distinct hexagonal pattern without any halo suggesting highly crystalline nature (S17b-c). Prominent D and G band after exfoliation ensures the structural integrity of the exfoliated graphene (Figure S17d). While, AFM proves the flake thickness is 1.2 nm or lower (Figure S17e). These indicates that the remaining unexfoliated graphite can again be exfoliated and the yield can be increased further.

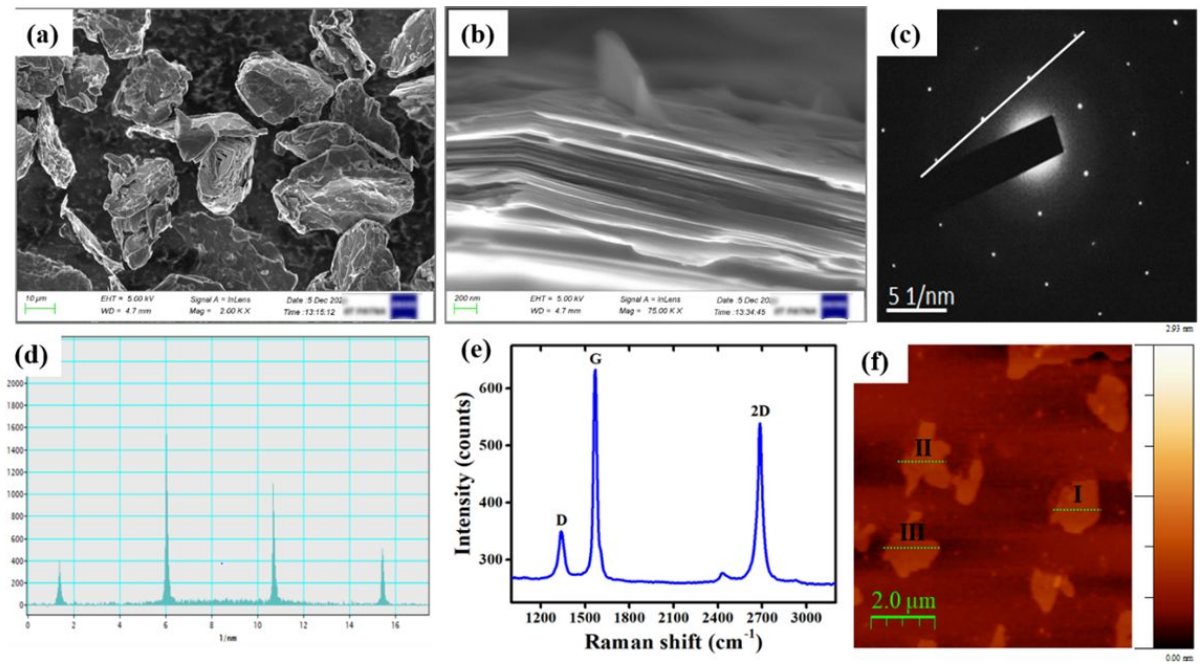

Figure S17: (a,b) Low and high magnification SEM, (c) SAED (d) intensity of line passing through (1–210)–(0–110)–(–1010)–(–2110) in figure S17c, (e) Raman and (e) AFM of exfoliated graphene obtained from the recycled graphite.

S18: Price calculation of exfoliated graphene

In order to commercialize this synthesized graphene, cost comparison of the same with the market-available graphene products becomes vital. During the whole processing and fabrication, a total of 20 g graphite (@ 120 g/h) was fed into the hot plasma for obtaining the exfoliated graphene. 1 run of the plasma spraying has been carried out for 10 minutes. Plasma gases were mainly Argon, as primary gas and Hydrogen, as secondary gas. Argon was also used as shroud gas during the whole process. Hence, the main cost obtained were comprised of: (a) cost of graphite, (b) cost of gases, (c) electricity costs and (d) manpower.

These various costs incurred during whole conversion process of graphite to graphene are provided below:

1) Price of synthetic graphite used (Sigma Aldrich): 94 USD/kg

Amount of graphite used = 120 g/h

Cost of graphite for 10 min (**C1**) = 0.094×10×2 = 1.88 USD

2) Cost of gases used (Praxair Inc.):

Three different gases were used for specific purpose during graphene preparation. Argon as primary gas as well as shroud gas and hydrogen as secondary gas.

(i) Price of Argon gas cylinder used for primary gas (capacity: 9486.14 litres) = 66.14 USD
Cost of Argon per litre = 0.0069 USD

(ii) Price of Hydrogen gas cylinder used (capacity: 5533.18 litres) = 238.09 USD
Cost of Hydrogen per litre = 0.043 USD

(iii) Price of Argon gas cylinder used for shroud gas (capacity: 9486.14 litres) = 66.14 USD
Cost of Argon per litre = 0.0069 USD

Table S18-1: Total cost calculation for gases:

Gases used	**Flow rate (SCFH)**	**Time (min.)**	**Total Vol. (Litre)**	**Cost/L (USD)**	**Total Cost (USD)**
Argon	120	10	566.3	0.0069	3.90
Hydrogen	6	10	28.3	0.043	1.21
Argon (Shroud)	15	10	70.8	0.0069	0.48
Total Cost for gases (**C2**)					**5.59**

Table S18-2: Cost of Energy consumption:

Cost of power per unit = 0.11 USD

Power (kW)	Time (hr)	Energy consumption (kWh)	Cost/unit (USD)	Total energy consumption cost in USD (C3)
39.7532	0.34	13.51	0.11	1.49

Cost of manpower: $0.041 (calculated tentatively for 1 gram)

Total amount of graphene produced = 8 g

Total cost in USD = **C1+C2+C3+C4**

= 1.88 + 5.59 + 1.49+ 0.04

= 9

Cost of 1g graphene = 9/8 = 1.12 USD

Please note that production cost depends upon the local condition (*i.e.* plasma gasses, electricity charge, labor cost *etc.*), Hence this estimated production cost may be taken as a reference. The cost can also vary based on the raw materials used. Use of natural graphite, which is much cheaper than synthetic graphite can lower down the production cost too. Below analysis provides the experimental and analytical evidences of exfoliation of natural graphite.

Natural graphite (NG) obtained from Sigma-Aldrich (Product ID: 808083) (Figure S18-1a). Scanning electron microscopy (SEM) shows the size of NG is 40-50 μm and are over 5 μm

thick (Figure S18-1b,c). The surface area of NG is 0.35 m^2/g (Figure S1S-1d). Raman spectra shows both the characteristics D and G band (Figure S18-1e). Figure S18-1f,g is the low magnification TEM image of NG and corresponding SAED pattern. High magnification TEM image of the NG shows numerous graphitic lattice planes stacked one over another with lattice spacing 0.34 nm (Figure S18-1h).

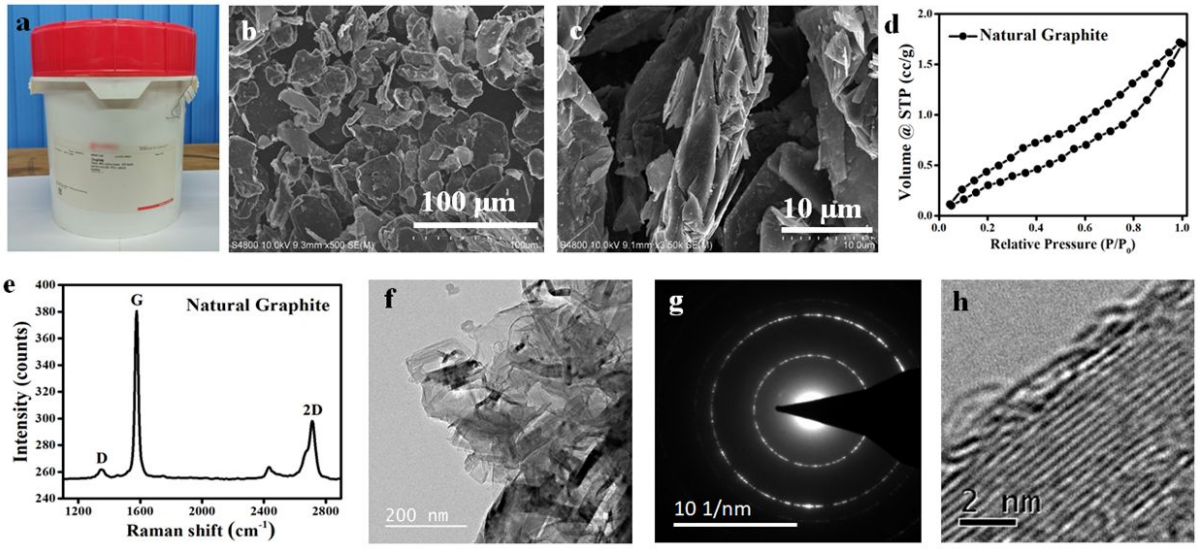

Figure S18-1: (a) Procured natural graphite powder, (b) SEM image of natural graphite flakes (c) cross-sectional view, (d) BET isotherm of natural graphite, (e) Raman Spectra of natural graphite, (f) low magnification image TEM image, (g) SAED pattern and (h) high magnification image showing lattice plane of natural graphite.

Exfoliation was carried out at parameters, Plasma power = 44 kW and primary gas flow rate = 120 SCFH. Higher power was needed to exfoliate the synthetic graphite due to the higher particle size of the natural graphite. Figure S18-2a shows the digital image of the exfoliated graphene dispersed in organic liquids (DMF and NMP). The exfoliated graphite remains suspended in these liquids for over 48 hours. The exfoliated graphene displays 93% reduction in intensity of X-Ray diffraction (002) peak intensity at $2\theta=26.5^{\circ}$ suggesting high degree of exfoliation (Figure S18-2b). Substantial increase in the surface area (634 m^2/g) was also observed for the exfoliated graphite (Figure S18-2c). The XRD and BET results are similar to

that of the synthetic graphene and confirms the successful exfoliation of natural graphite to graphene.

Raman spectra of the exfoliated graphite shows prominent D and G band suggesting structural integrity after plasma spraying (Figure S18-2d). The 2D band is sharp and symmetric similar to single layer graphene and can be distinguished from that of graphite (Figure S19-2e). The XPS results (Figure S18-2f, g) shows that the atomic ratio of carbon and oxygen (C/O) is 26.6%, which is similar to that of the synthetic graphene. XPS was performed using a X-ray photoelectron spectroscopy (PHI 5000 Versa Prob II, FEI Inc., USA). Figure S18-2h shows the low magnification TEM image of the exfoliated graphene. A bright edge without noticeable dark line is the characteristics of single layer graphene (Figure S18-2i). The SAED pattern shown as inset in Figure S18-2i is representative of highly crystalline nature of the exfoliated graphene. Atomic resolution inverse fourier image shows perfect hexagonal pattern for the single layer graphene (Figure S18-2j).

SEM images shows that the lateral dimensions of the flakes are between 2 to 4 μm (Figure S18-2k). AFM proves that the flakes are 1 nm thick or less, providing evidence of single layer to few layers graphene (Figure S18-2l). The dynamic light scattering result shown in Figure S18-2m supports the previous results indicating that the natural graphite has been exfoliated successfully to graphene.

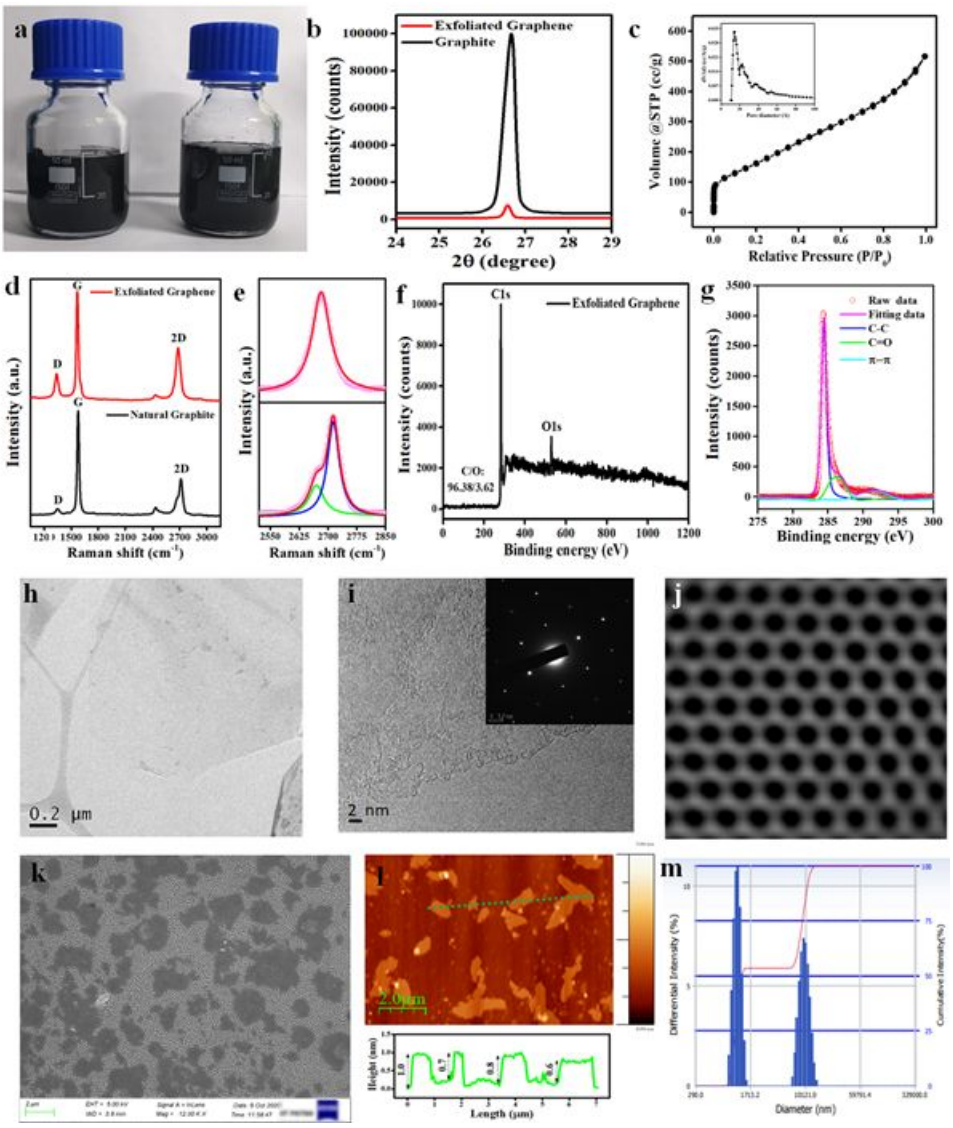

Figure S18-2: (a) Stable dispersion of exfoliated NG in DMF (left) and NMP (right)(Concentration: 5 mg/mL), (b) XRD, (c), BET and pore size (inset), (d) Raman spectra, (e)2D band structure of exfoliated graphene and natural graphite, (f) Survey and (g) core-level carbon 1s XPS spectra of graphene, (h) TEM image of single layer graphene, (i) high magnification image from edge of the single layer graphene, SAED (inset), (j) IFFT showing perfect honeycomb structure, (k) SEM, (l) AFM and height profile and (m) DLS of exfoliated graphene.

S19: Comparison of achieved results with literatures

The fulfilment of four essential factors, *i.e*., (1) high quality (2) narrow layer distribution (3) fast and reproducible technique and (4) high throughput is necessary for synthesizing quality graphene for various applications. So far no studies have reported the simultaneous fulfilment of these 5 factors. We compiled list of few notable works of graphene synthesis (2007 to Present) and compared them with our plasma spray exfoliated graphene. Comparisons were made for 7 sectors: Medium used, layer numbers, I_D/I_G (from Raman), C/O and sp^2 % (from XPS), production rate and yield %.

Table S19: List of papers describing synthesis of graphene using different routes. Comparisons were drawn on various factors including medium used, layer numbers, I_D/I_G, C/O and sp^2 %, production rate and yield %.

Sl No	Reference	Methods	Medium used	Number of Graphene Layers	I_D/I_G	C/O (ratio)	sp^2 (%)	Production Rate (g/h)	Yield %
1	**Current Work**	**Plasma spraying**	**No Chemicals**	**1-3 layer**	**0**	**95.5/4.5**	**95**	**48 g/h**	**40%**
2	Loung *et al*. Nat. [84]	Flash Technique	No solvent	Turbostratic graphene	~0	65/25	98.6	--	80-90%
3	Kwon *et.al*. Adv. Mat. Int. [85]	Electrochemical Exfoliation	$(NH_4)_2SO_4$	Few layer <10 layer	0.14	16.2	36.0	30.0	--
4	Dominguez *et.al*. Nat. prot. [86]	Ball Milling	Melamine	3-4 layer	0.2-0.5	91.0/7.7	--	--	--
5	Ejigu *et al*. Adv. Funct. Mater. [87]	Electrochemical Exfoliation	$CoSO_4$ and Na_2SO_4	Few layer < 5 layer	0.05	36	--	--	--

6	Buzaglo *et al*. Adv. Mater. [88]	Ball Milling	naphthalene, anthracene and pyrene	Graphene <10 layer	0.15-0.75	--	55-75	--	>90%
7	Buzaglo *et al*. Chem. Mater. [89]	Sonication	Water	Few layer >5 layer	0.13-0.50	--	85-92	--	<14%
8	Voiry *et.al*. Science [90]	Microwave reduction	NA	1-3 layer	0	--	90	--	--
9	Yang *et.al*. J. Am. Chem. Soc. [91]	Electrochemical Exfoliation	$(NH_4)_2SO_4$	Few layer < 5 layer	<0.1	~25.3	--	--	45%
10	Paton *et al*. Nat. Mater. [92]	Shear exfoliation	NMP, NaC *etc.*	Few layer <10 layer	0.4	--	--	5.3	3%
11	Matsumoto *et al*. Nat. Chem. [93]	Microwave irradiation	oligomeric ionic liquids	Mono layer	0.14	~30	--	--	93%
12	Parvez *et al*. J. Am. Chem. Soc. [94]	Electrochemical Exfoliation	$(NH_4)_2SO_4$, Na_2SO_4, K_2SO_4 *etc.*	Few layer ≤ 3 layer	0.42	~17.2	--	--	>85%
13	Du *et al*. J. Mater. Chem. A [95]	liquid-phase exfoliation	NMP,DMF	1-5 layer	0.4	--	--	0.1-2	<95%
14	Leon *et al*. ACS Nano [96]	Ball milling	Aminotriazine	Few layer <5 layer	0.4-0.8	--	--	--	--
15	Geng *et al*. Sci. Rep. [97]	Catalytic exfoliation	FeCl3 and H_2O_2	Few layer <5 layer	0.1	--	--	--	--
16	Yang *et al*. Carbon [98]	Sonication	Water, Py-1SO_3	Few layer <7 layer	0.8	~14%	--	--	70%
17	You *et al*. Carbon [99]	Hummer's method	Water, alcohol *etc*.	>10 layer	1.1	2.85	~60	--	>65%

18	Zhang *et al*. Carbon [100]	Thermal exfoliation	NA	1-10 layer	--	9.8-15.6	--	--	--
19	Liao *et al*. Carbon [101]	Sonication	NMP	Few layer <10 layer	0.5	--	--	--	15%
20	Lu *et al*. J. Mater. Chem. [102]	Sonication	chlorosulfonic acid and H_2O_2	Few layer >5 layer	~0.1	--	--	0.25 g/h	--
21	Herron *et al*. J. Mater. Chem. [103]	CVD	NA	Few Layer <5 layer	~1.2	--	--	--	--
22	Ang *et al*. ACS Nano [104]	Hummer's method	NA	Monolayer	1.2	40-50	--	--	>90%
23	Choi *et al*. Nanotechnol. [105]	Mild sonication	1-propanol	1-5 layer	0.6	~80	--	0.015 g/h	--
24	Knieke *et al*. Carbon [106]	Mechanical delamination (wet grinding)	anionic surfactant sodium dodecyl sulfate	Multilayer >10 layer	0.6	--	--	1.5-2.5 g/h	--
25	Zhu *et al*. ACS Nano [107]	Bath Sonication	Propylene Carbonate	Graphene >10 layer	~1.0	--	--	--	--
26	Gu *et al*. J. Mater. Chem. [108]	Liquid phase exfoliation	H_2SO_4 and H_2O_2	1-3 Layer	0.2	--	--	--	--
27	Hernandez *et al*. Nat. Nanotechnol. [109]	liquid-phase exfoliation	N-methyl-pyrrolidone NMP	1 layer	~0.4	--	--	1 wt.% Not in g/h	0.83 %

28	Stankovich *et al*. Carbon [110]	chemical reduction	hydrazine hydrate	Few layer < 5 layer	1.2	--	--	--	--
29	Shang *et al*. Adv. Funct. Mater. [111]	CVD	Edge termination by C(O)OH	Multilayer Graphene	-	-	-	~ 1g/h	--
30	Allen *et al*. Chem. Com. [112]	Chemically Induced folding	Ethanol	Few layer <5 layer	1.0	55	--	0.9 g/h	--

S20: Reproducibility of exfoliated graphene

Now, after the successful large scale fabrication of high quality, defect free single layer graphene with ~15% of bi-/tri- layer, it is necessary to ensure the reproducibility of the single layer. Hence, keeping the parameters constant *i.e*., (40 kW, 120 SCFH), five different batches were plasma sprayed to obtain graphene (Figure S20-1). About 4 grams of graphene were obtained in each batch in 6 minutes.

After preparation of the graphene, we performed the preliminary analysis *viz.* Raman and AFM separately for all batches. It was found that all the batches have almost similar characteristics. Raman spectra of all five batches of graphene samples show G and 2D peaks at ~1580 and 2719 cm^{-1} respectively. AFM analyses of ~50 flakes revealed that 75-85 % of flakes were single layer (Figure S20-2). This result indicates that the results are reproducible for a constant parameter.

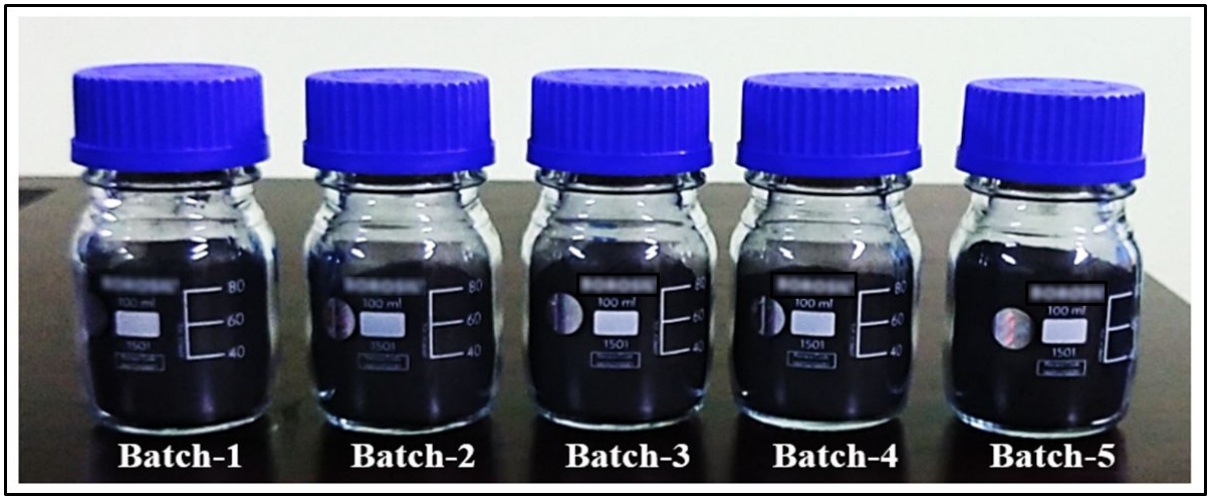

Figure S20-1: The digital images of five different batch (B1-B5) of graphene powder

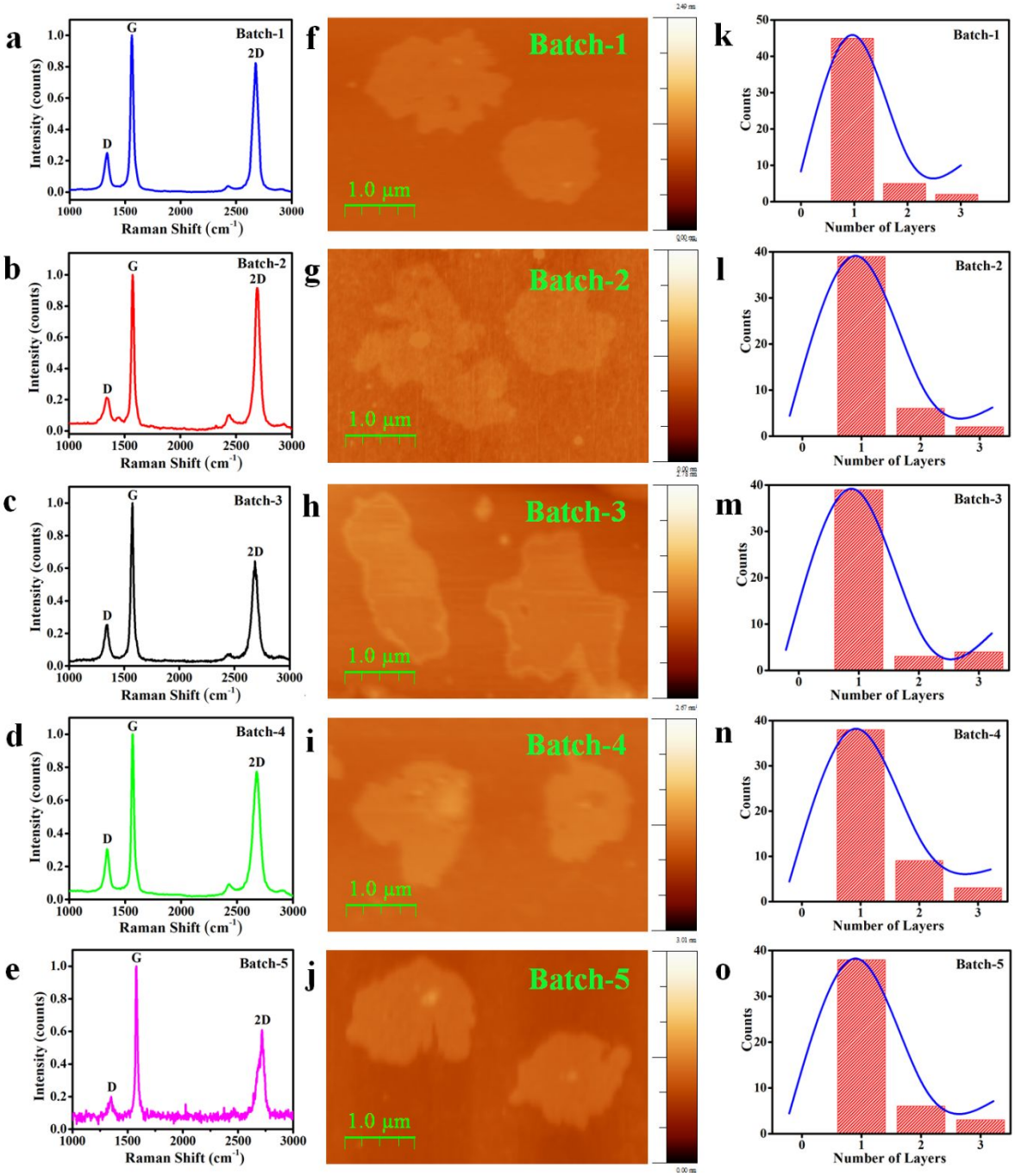

Figure S20-2: (a-e) Raman spectra, (f-j) AFM images and (k-o) layer distribution of the five different batches of graphene samples respectively.

S21: Experimental details on proof-of-concept of exfoliated graphene

S21a: Layer-wise Young's modulus of exfoliated graphene

We used an AFM force-indention (Model: MFP-3D, Asylum Research, USA) to obtain the force *vs*. deflection traces (curve). The exfoliated graphene was dispersed in ethanol and drop-casted over a clean ITO surface (Techscience Services Pvt. Ltd., India). Figure S21-1a shows the SEM image of a graphene deposited flake over ITO substrate. The valley and ridge like feature of the ITO surface provides a situation analogous to graphene suspended over pillars. The schematic of the indentation experiment is shown in Figure S21-1b. Firstly, the ITO surface was scanned for graphene flakes using AFM in tapping mode. The layers of the graphene flakes were measured based on its thickness. At least two AFM scans were carried out to endorse that no drift occurred on the graphene during indentation.

The AFM tip was placed directly at the centre of two ridges and load of 10nN was applied. As the load was applied the graphene flake moved downward, the linear force *versus* indentation depth/deflection (F-h) was extrapolated (Figure S21-1c). The elastic modulus for a single indentation curve was evaluated by applying an extension of the Oliver Pharr model taking into account the effect of adhesion. The four-sided pyramid shaped AFM probe tip was modelled by a cone geometry (a cone angle around 22°) for elastic modulus determination. The Young's modulus distribution was obtained from values calculated for all force curves in a force map (20 μm × 20 μm). At least fifty cycles of loading and unloading were performed on the same graphene flake. Among them, five of loading and unloading curves were shown in Figure S21-1c. The extension and retraction curves indicate high elasticity of graphene flakes. The distribution of Young's modulus is presented in the main manuscript and values are comparable with the literature.[113-118]

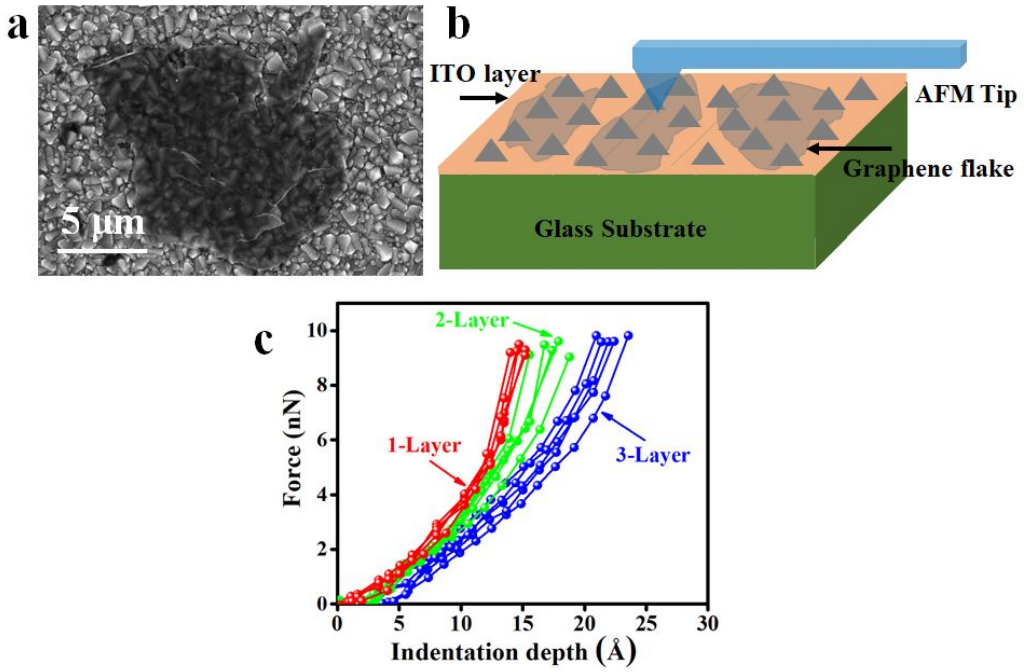

Figure S21-1: (a) FESEM images showing suspended graphene flakes over ITO substrate, (b) Schematics showing experimental setup of indentation over suspended graphene flakes with an AFM tip. (c) Force-deflection curves of 1-3-layer graphene flake at 10 nN loads.

S21b: Tribological test on exfoliated graphene coated substrate

Ethanol solution containing exfoliated graphene (1mg/mL) was spread on the highly polished surfaces of the Si wafer (Techscience Services Pvt. Ltd., India) using spin coating. Prior to spin coating, the flat samples of Si substrates were cleaned by sonication in de-ionized water and acetone to remove any surface contaminations. The graphene coated substrate was evaporated in a dry environment for better adherence of the flakes. Tribological studies of the coated samples were performed against a 3 mm diameter steel ball using a ball on disc tribometer (Ducom Pvt. Ltd, India). The schematic of the experimental setup is shown in Figure S21-2a. All tests were performed at room temperature. Normal load of 1, 2 and 3 N was used during the tests. Sliding speed of 60 rpm was maintained throughout the tests. All tests were run for

1800 cycles. The tribo test result (COF) obtained using 2N and 3N is shown in Figure S21-2b and S21-2c respectively, while the value obtained using 1N is shown in the main manuscript. All the tests show COF lower than 0.03 representing very low value, for graphene-steel interaction, comparable to the literature.[119-121]

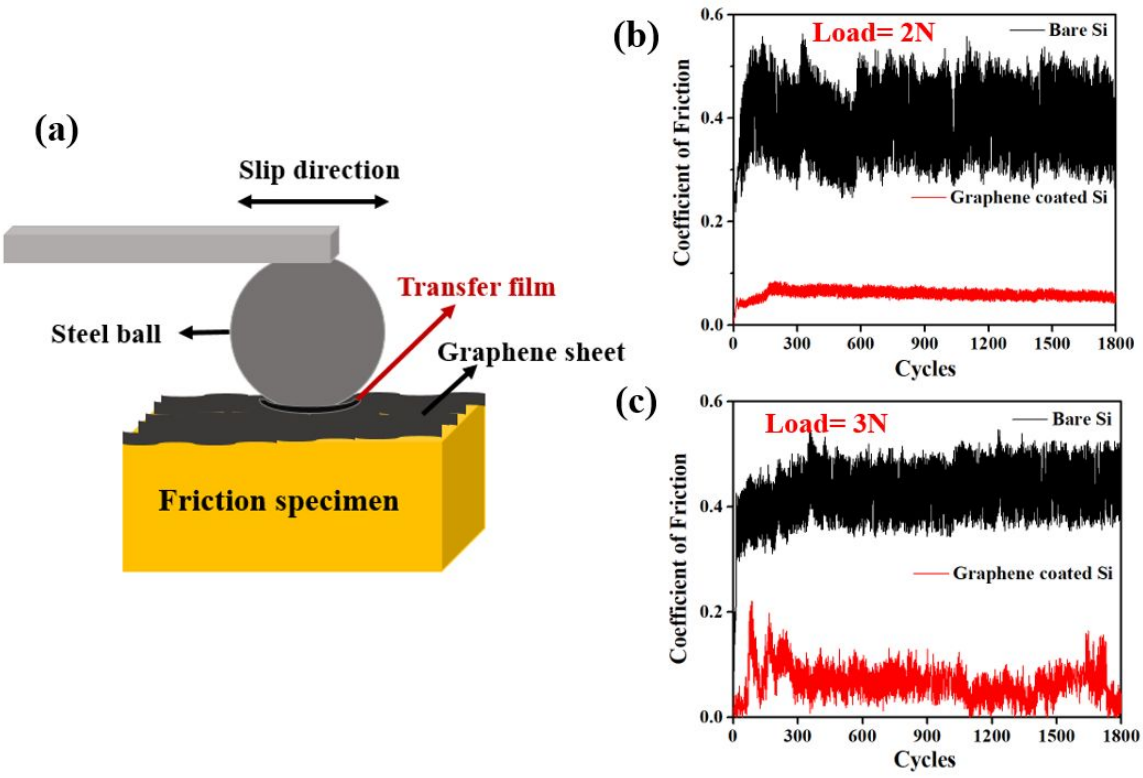

Figure S21-2: (a) Schematic of the experimental setup, COF curves obtained using load (b) 2N and (c) 3N.

S21c: Electrical conductivity of exfoliated graphene

All the electrical conductivity measurements were done using a conductive Atomic Force Microscope (C-AFM) (Asylum/Oxford Instruments, MFP3D Origin, USA). Firstly, the exfoliated graphene was deposited over a conductive substrate (ITO) using spin-coating. Before measuring the conductivity of graphene flakes, height profiles were grabbed to identify the graphene layers (based on thickness) in non-contact mode as shown in Figure 22-3a-c.

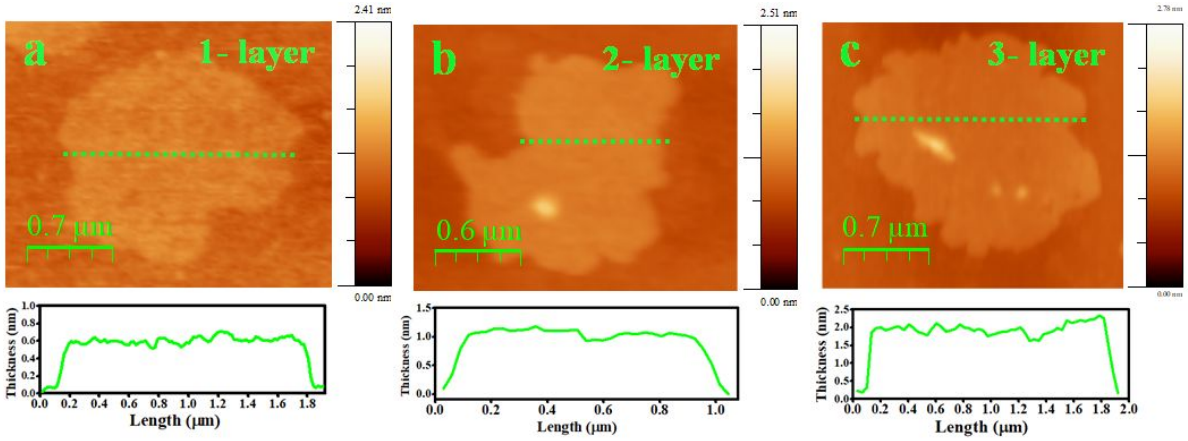

Figure S21-3: Identification of 1 layer, 2 layers, and 3 layers graphene sheets by AFM.

Then the sample surface was scanned for conductivity measurement in contact-mode. To measure the local conductance of the graphene film, sample was biased with different voltages. All the measurements were performed under room temperature conditions. The schematics of the experimental setup is shown in figure S21-4a. Figure S21-4b-d shows the optical microscope image of the graphene flakes deposited over the ITO substrate, whereas the marked area in Figure S21-4e-g is the cantilever tip approaching the flakes. All AFM measurements were performed at 512 × 512 resolution and a scanning area of a 2 × 2 μm^2. A cross filter was placed to lessen the background noise in the data. The conductivity measurements were done on ~50 points at the centre of the graphene flake profile and were averaged for the analysis.[122]

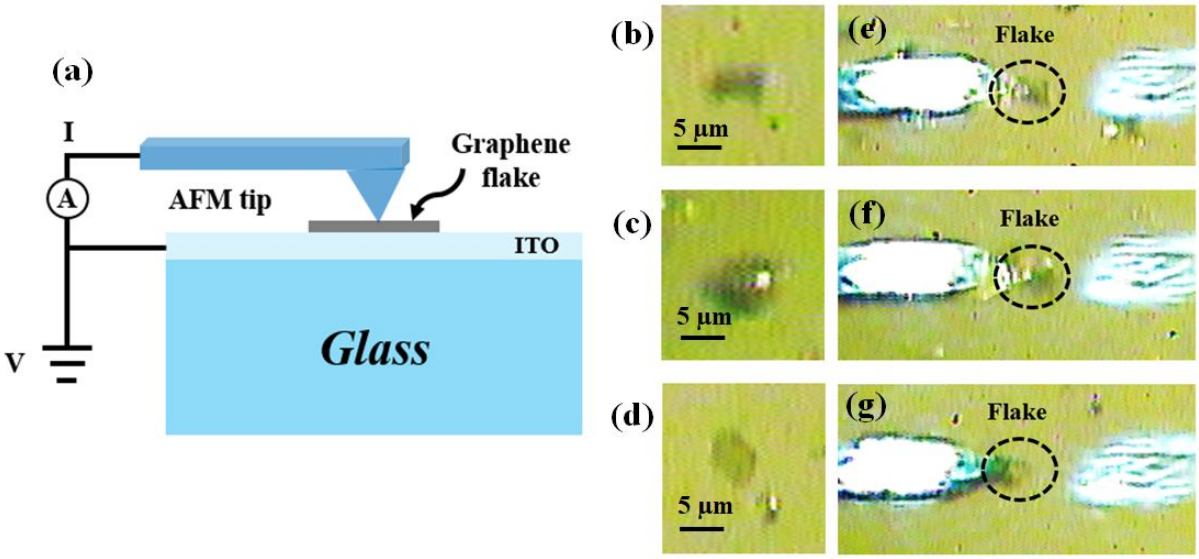

Figure S21-4: (a) schematic of the experimental setup for C-AFM and (b,c,d) shows the optical microscope image of the graphene flakes deposited over substrate, whereas the marked area in (e,f,g) is the cantilever tip approaching the flakes.

S21d: Transmittance test on exfoliated graphene coated substrate

The optical measurement of exfoliated graphene film was done using a UV-Visible/NIR spectrophotometer (Jasco V-770). The exfoliated graphene flakes were uniformly dispersed in Dimethylformamide (DMF) and then spin coated over a quartz substrate. The sample was dried at 120°C for over-night in hot air oven. For understanding the dependencies of transmittance of the graphene film, the percentage of transmittance was studied.

The thickness of the graphene film was measured to be ~50 nm (Figure S21-5a)

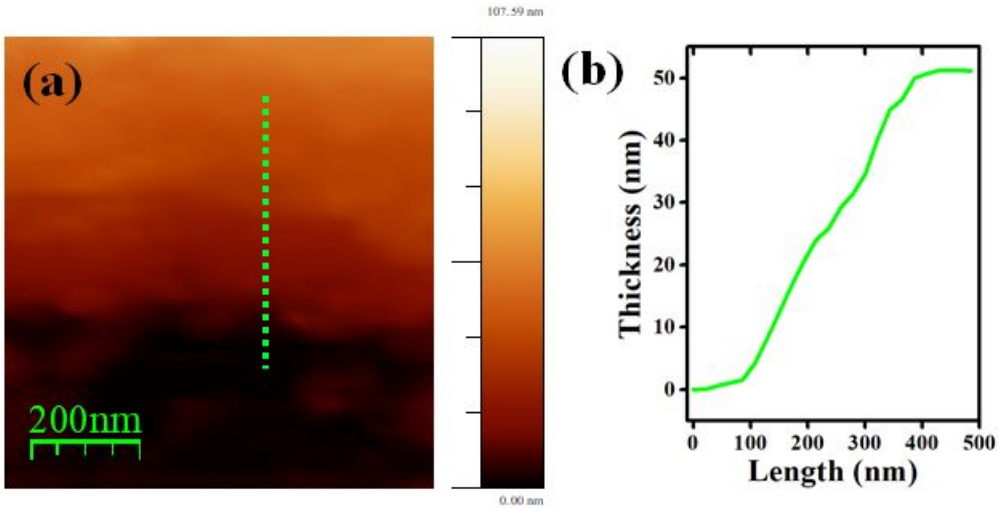

Figure S21-5a: (a) AFM of the graphene film depicting film thickness, (b) line profile along the dotted line in figure S21-5a

The graphene film was also uniform over a large area. In order to demonstrate the uniformity of the coating, AFM was done over the surface of the film. Figure S21-5b-a is the AFM image of scanned area (500 μm^2). The corresponding line profile along the surface (depicted by green

dotted line) gives roughness of only ±5 nm, proving uniformity of the graphene film (Figure S21-5b-b).

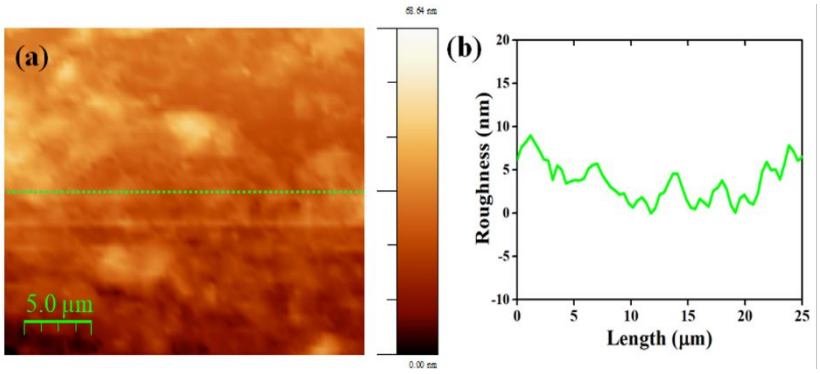

Figure S21-5b: (a) AFM over graphene film, (b) line profile for the green dotted area in previous figure.

S21e: Electrochemical test of exfoliated graphene

For electrochemical measurements 4 mg of active material was dispersed in 2 ml of NMP and slurry was deposited on glassy carbon electrode. The mass loading of active material on the electrode was 20 µg. The electrode was dried at room temperature before electrochemical tests. Cyclic voltammetry (CV) measurements were performed by the Potentiostat/Galvanostat/FRA (Interface 1000, Gamry, USA) in a three electrode configuration with Ag/AgCl as the reference electrodein 0.5 M Na_2SO_4 aqueous electrolyte. Platinum (Pt) electrode was used as the counter electrode. Data analysis of the curves was done using the Electro Chem software supplied along with the equipment.

Cyclic voltammetry (CV) experiment were performed for eight different scan rates (5, 10, 20, 50, 100, 200, 300 and 500 mV s^{-1}) in the potential window from 0 to +1 V. The CV characteristics at different scan rate for exfoliated graphene is shown in main manuscript while the curves obtained for graphite is shown here (Figure S21-6a). The specific capacitance was calculated from CV curves according to the following equation.[123,124]

$$C_{sp} = \frac{\int Id\vartheta}{\Delta V \times m \times s} \qquad [4]$$

Where, C_{sp} (F/g) is the specific capacitance, $\int Id\vartheta$ is the integrated area under the CV curve, m (g) is the mass of active material deposited on electrode surface, ΔV (V) is the difference in potential, and s is the potential scan rate. The specific capacitance at scan rate 5, 10, 20, 50, 100, 200, 300 and 500 mV s^{-1} are 375, 347, 335, 311, 294, 287, 268 and 249 F/g respectively. The maximum specific capacitance was 375 F/g at scan rate 5 mV s^{-1}.

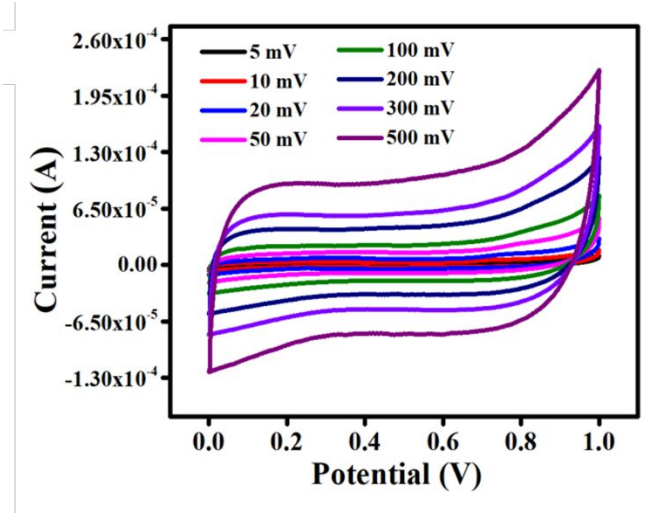

Figure S21-6: Comparison of CV characteristics of graphite at different scan rate.

Galvanostatic charge–discharge experiments were also used to calculate the specific capacitance using the following equation, [125,126]

$$C_{sp} = \frac{I}{m} \times \frac{dt}{d\vartheta} \qquad [5]$$

where C_{sp} (F/g)is the specific capacitance, I (A), is the constant current, dt is the discharging time (s), m is the mass of active material deposited on electrode surface (g) and $d\vartheta$ is the voltage change in charge–discharge process. The specific capacitance obtained from galvanostatic charge/discharge curves are 348, 284, 211, 203 and 124 F/g for current density 0.75, 1.0, 1.5, 2.0, 5.0 A/g.

REFERENCES

1. Tour, J. M. Top-Down *versus* Bottom-Up Fabrication of Graphene-Based Electronics, *Chem. Mater.* **2014**, 26, 163-171.
2. Neumann, C.; Kaiser, D.; Mohn, M. J.; Füser, M.; Weber, N. E.; Reimer, O.; Gölzhäuser, A.; Weimann, T.; Terfort, A.; Kaiser, U.; Turchanin, A. Bottom-Up Synthesis of Graphene Monolayers with Tunable Crystallinity and Porosity. *ACS Nano* **2019**, 13, 7310-7322.
3. Omiciuolo, L.; Hernández, E. R.; Miniussi, E.; Orlando, F.; Lacovig, P.; Lizzit, S.; Menteş, T. O.; Locatelli, A.; Larciprete, R.; Bianchi, M.; Ulstrup, S.; Hofmann, P.; Alfè, D.; Baraldi, A. Bottom-Up Approach for the Low-Cost Synthesis of Graphene-Alumina Nanosheet Interfaces Using Bimetallic Alloys. *Nat. Commun.* **2014,** 5, 5062.
4. Tang, L.; Li, X.; Ji, R.; Teng, K. S.; Tai, G.; Ye, J.; Wei, C.; Lau, S. P. Bottom-Up Synthesis of Large-Scale Graphene Oxide Nanosheets. *J. Mater. Chem.* **2012**, 22, 5676.
5. Tomai, T.; Nakayasu, Y.; Okamura, Y.; Ishiguro, S.; Tamura, N.; Katahira, S.; Honma, I. Bottom-Up Synthesis of Graphene *via* Hydrothermal Cathodic Reduction. *Carbon* **2020**, 158, 131-136.
6. Jiang, L.; Niu, T.; Lu, X.; Dong, H.; Chen, W.; Liu, Y.; Hu, W.; Zhu, D. Low-Temperature, Bottom-Up Synthesis of Graphene *via* a Radical Coupling Reaction. *J. Am. Chem. Soc.* **2013**, 135, 9050-9054.
7. Reina, A.; Jia, X.; Ho, J.; Nezich, D.; Son, H.; Bulovic, V.; Dresselhaus, M. S.; Kong, J. Large Area, Few-Layer Graphene Films on Arbitrary Substrates by Chemical Vapor Deposition. *Nano Lett.* **2009**, 9, 30-35.
8. Banszerus, L.; Schmitz, M.; Engels, S.; Dauber, J.; Oellers, M.; Haupt, F.; Watanabe, K.; Taniguchi, T.; Beschoten, B.; Stampfer, C. Ultrahigh-Mobility Graphene Devices from Chemical Vapor Deposition on Reusable Copper. *Sci. Adv.* **2015**, 1, 1500222.
9. Chae, S. J.; Gunes, F.; Kim, K. K.; Kim, E. S.; Han, G. H.; Kim, S. M.; Shin, H. J.; Yoon, S. M.; Choi, J. Y.; Park, M. H.; Yang, C. W.; Pribat, D.; Lee, Y. H. Synthesis of Large-Area Graphene Layers on Poly-Nickel Substrate by Chemical Vapor Deposition: Wrinkle Formation. *Adv. Mater.* **2009**, 21, 2328-2333.
10. Lin, W. H.; Chen, T. H.; Chang, J. K.; Taur, J. I.; Lo, Y. Y.; Lee, W. L.; Chang, C. S.; Su, W. B.; Wu, C. I. A Direct and Polymer-Free Method for Transferring Graphene Grown by Chemical Vapor Deposition to Any Substrate. *ACS Nano* **2014**, 8, 1784-1791.

11. Shi, Q.; Tokarska, K.; Ta, H. Q.; Yang, X.; Liu, Y.; Ullah, S.; Liu, L.; Trzebicka, B.; Bachmatiuk, A.; Sun, J.; Fu, L.; Liu, Z.; Rümmeli, M. H. Substrate Developments for the Chemical Vapor Deposition Synthesis of Graphene. *Adv. Mater. Interfaces* **2020**, **7**, 1902024.

12. Plutnar, J.; Pumera, M.; Sofer, Z. The Chemistry of CVD Graphene. *J. Mater. Chem. C.* **2018**, 6, 6082-6101.

13. Polat, E. O.; Balci, O.; Kakenov, N.; Uzlu, H. B.; Kocabas, C.; Dahiya, R. Synthesis of Large Area Graphene for High Performance in Flexible Optoelectronic Devices. Sci. Rep. **2015**, 5, 16744.

14. Lin, L.; Peng, H.; Liu, Z. Synthesis Challenges for Graphene Industry. *Nat. Mater.* **2019**, 18, 520-529.

15. Bonaccorso, F.; Lombardo, A.; Hasan, T.; Sun, Z.; Colombo, L.; Ferrari, A. C. Production and Processing of Graphene and 2D Crystals. *Materials Today.* **2012**, 15, 564-589.

16. Dato, A.; Radmilovic, V.; Lee, Z.; Phillips, J.; Frenklach, M. Substrate-Free Gas-Phase Synthesis of Graphene Sheets. *Nano Lett.* **2008**, 8, 2012-2016.

17. Jo, E. H.; Chang, H.; Kim, S. K.; Choi, J. H.; Park, S. R.; Lee, C. M.; Jang, H. D. One-Step Synthesis of Pt/Graphene Composites from Pt Acid Dissolved Ethanol *via* Microwave Plasma Spray Pyrolysis. *Sci. Rep.* **2016**, 6, 33236.

18. Hu, Y.; Jensen, J. O.; Zhang, W.; Huang, Y.; Cleemann, L. N.; Xing, W.; Bjerrum, N. J.; Li, Q. Direct Synthesis of Fe_3C-Functionalized Graphene by High Temperature Autoclave Pyrolysis for Oxygen Reduction. *Chem. Sus. Chem.* **2014**, 7, 2099-2103.

19. Zhang, H.; Cao, T.; Cheng, Y.; Preparation of Few-Layer Graphene Nanosheets by Radio-Frequency Induction Thermal Plasma. *Carbon* **2015**, 86, 38-45.

20. Lim, S.; Shimizu, A.; Yoon, S. H.; Korai, Y.; Mochida, I. High Yield Preparation of Tubular Carbon Nanofibers Over Supported Co-Mo Catalysts. *Carbon* **2004**, 42, 1279-1283.

21. Yang, J.; Liao, Q.; Zhou, X.; Liu, X.; Tang, J. Efficient Synthesis of Graphene-Based Powder *via in Situ* Spray Pyrolysis and Its Application in Lithium Ion Batteries. *RSC Adv.* **2013**, 3, 16449-16455.

22. Webb, M. J.; Palmgren, P.; Pal, P.; Karis, O.; Grennberg, H. A Simple Method to Produce Almost Perfect Graphene on Highly Oriented Pyrolytic Graphite. *Carbon* **2011**, 49, 3242-3249.

23. Wang, C.; Sun, L.; Dai, X.; Li, D.; Chen, X.; Xia, W.; Xia, W. Continuous Synthesis of Graphene Nano-Flakes by a Magnetically Rotating Arc at Atmospheric Pressure. *Carbon* **2019**,148, 394-402.

24. Shin, Y. C.; Kong, J. Hydrogen-Excluded Graphene Synthesis *via* Atmospheric Pressure Chemical Vapor Deposition. *Carbon* **2013**, 59, 439-447.

25. Lin, Z.; Waller, G. H.; Liu, Y.; Liu, M.; Wong, C. 3D Nitrogen-Doped Graphene Prepared by Pyrolysis of Graphene Oxide with Polypyrrole for Electrocatalysis of Oxygen Reduction Reaction. *Nano Energy* **2013**, 2, 241-248.

26. Kwak, J.; Chu, J. H.; Choi, J. K.; Park, S. D.; Go, H.; Kim, S. Y.; Park, K.; Kim, S. D.; Kim, Y. W.; Yoon, E.; Kodambaka, S.; Kwon, S. Y. Near Room-Temperature Synthesis of Transfer-Free Graphene Films. *Nat. Commun.* **2012**, 3, 645.

27. Kamalakaran, R.; Terrones, M.; Seeger, T.; Redlich, P. K.; Ruhle, M. Synthesis of Thick and Crystalline Nanotube Arrays by Spray Pyrolysis. *Appl. Phys. Lett.* **2000**, 77, 3385-3387.

28. Lee, S. W.; Mattevi, C.; Chhowalla, M.; Sankaran, R. M. Plasma-Assisted Reduction of Graphene Oxide at Low Temperature and Atmospheric Pressure for Flexible Conductor Applications. *J. Phys. Chem. Lett.* **2012**,3, 772-777.

29. Lee, B. J.; Cho, S. C.; Jeong, G. H. Atmospheric Pressure Plasma Treatment on Graphene Grown by Chemical Vapor Deposition. *Current Applied Physics* **2015**, 15, 563-568.

30. Bundaleska, N.; Tsyganov, D.; Dias, A.; Felizardo, E.; Henriques, J.; Dias, F. M.; Abrashev, M.; Kissovski, J.; Tatarova, E. Microwave Plasma Enabled Synthesis of Free Standing Carbon Nanostructures at Atmospheric Pressure Conditions. *Phys. Chem. Chem. Phys.* **2018**, 20, 13810.

31. Li, M.; Liu, D.; Wei, D.; Song, X.; Wei, D.; Wee, A. T. S. Controllable Synthesis of Graphene by Plasma-Enhanced Chemical Vapor Deposition and Its Related Applications. *Adv. Sci.* **2016**,3, 1600003.

32. Yeh, N. C.; Hsu, C. C.; Bagley, J.; Tseng, W. S. Single-Step Growth of Graphene and Graphene-Based Nanostructures by Plasma Enhanced Chemical Vapor Deposition. *Nanotechnology* **2019**, 30, 162001.

33. Cai, M.; Thorpe, D.; Adamson, D. H.; Schniepp, H. C. Methods of Graphite Exfoliation. *J. Mater. Chem.* **2012**, 22, 24992-25002.

34. Ciesielsk, A.; Samori, P. Graphene *via* Sonication Assisted Liquid-Phase Exfoliation. *Chem. Soc. Rev.* **2014**, 43, 381-398.

35. Hong, Y.; Wang, Z.; Jin, X. Sulfuric Acid Intercalated Graphite Oxide for Graphene Preparation. *Sci. Rep.* **2013**, 3, 3439.

36. Liu, F.; Wang, C.; Sui, X.; Riaz, M. A.; Xu, M.; Wei, L.; Chen, Y. Synthesis of Graphene Materials by Electrochemical Exfoliation: Recent Progress and Future Potential. *Carbon Energy.* **2019**, 1, 173-199.

37. Wang, X.; Wang, Y.; Zhao, C.; Zhao, Y.; Yan, B.; Zheng, W. Electrodeposited $Ni(OH)_2$ Nanoflakes on Graphite Nanosheets Prepared by Plasma-Enhanced Chemical Vapor Deposition for Supercapacitor Electrode. *New J. Chem.* **2012**, 36, 1902-1906.

38. Kim, J.; Suh, J. S. Size-Controllable and Low-Cost Fabrication of Graphene Quantum Dots Using Thermal Plasma Jet. *ACS Nano* **2014**,8, 4190-4196.

39. Ma, X.; Li, S.; Hessel, V.; Lin, L.; Meskers, S.; Gallucci, F. Synthesis of Luminescent Carbon Quantum Dots by Microplasma Process. *Chem. Eng. Process.* **2019**, 140, 29-3530.

40. Ang, P. K.; Wang, S.; Bao, Q.; Thong, J. T. L.; Loh, K. P. High-Throughput Synthesis of Graphene by Intercalation-Exfoliation of Graphite Oxide and Study of Ionic Screening in Graphene Transistor. *ACS Nano* **2009**, 3, 3587-3594.

41. Kim, K. S.; Seo, J. H.; Nam, J. S.; Ju, W. T.; Paek, K. H.; Hong, S. H. Production of Hydrogen and Carbon Black by Methane Decomposition Using DC-RF Hybrid Thermal Plasmas. *IEEE T Plasma Sci.* **2005**, 33, 813-823.

42. Choi, S. I.; Nam, J. S.; Lee, C. M.; Choi, S. S.; Kim, J. I.; Park, J. M.; Hong, S. H. High Purity Synthesis of Carbon Nanotubes by Methane Decomposition Using an Arc-Jet Plasma. *Curr. Appl. Phys.* **2006**,6**,** 224-229.

43. Choi, S. I.; Nam, J. S.; Kim, J. I.; Hwang, T. H.; Seo, J. H.; Hong, S. H. Continuous Process of Carbon Nanotubes Synthesis by Decomposition of Methane Using an Arc-Jet Plasma. *Thin Solid Films* **2006**,506, 244-249.

44. Zhang, H.; Cao, T.; Cheng, Y. Preparation of Few-Layer Graphene Nanosheets by Radio-Frequency Induction Thermal Plasma. *Carbon* **2015**, 86, 38-45.

45. Hong, Y.; Wang, Z.; Jin, X. Sulfuric Acid Intercalated Graphite Oxide for Graphene Preparation. *Sci. Re*p. **2013**, 3, 3439.

46. Fronczak, M.; Fazekas, P.; Károly, Z.; Hamankiewicz, B.; Bystrzejewski, M. Continuous and Catalyst Free Synthesis of Graphene Sheets in Thermal Plasma Jet. *Chem. Eng*. **2017**, 322, 385-396.

47. Tryba, B.; Morawski, A. W.; Inagaki, M. Preparation of Exfoliated Graphite by Microwave Irradiation. *Carbon* **2005**, 43, 2397-2429.

48. Lin, L.; Wang, Q. Microplasma: A New Generation of Technology for Functional Nanomaterial Synthesis. *Plasma Chem. Plasma Process.* **2015**, 35, 925-962.

49. Rhodes, D.; Chae, S. H.; Palau, R. R.; Hone, J. Disorder in *van der Waals* Heterostructures of 2D Materials. *Nat. Mater.* **2019**, 18, 541-549.

50. Wei, W.; Guan, T.; Li, C.; Shen, L.; Bao, N. Heating Rate-Controlled Thermal Exfoliation for Foldable Graphene Sponge. *Ind. Eng. Chem. Res.* **2020**, 59, 2946-2952.

51. Zhang, H. B.; Wang, J. W.; Yan, Q.; Zheng, W. G.; Chen, C.; Yu, Z. Z. Vacuum-Assisted Synthesis of Graphene from Thermal Exfoliation and Reduction of Graphite Oxide. *J. Mater. Chem.* **2011**, 21, 5392-5397.

52. Kwak, H. S.; Uhm, H. S.; Hong, Y. C.; Choi, E. H. Disintegration of Carbon Dioxide Molecules in a Microwave Plasma Torch. *Sci. Rep.* **2015**, 5, 18436.

53. Fenimore, C. P.; Jones, C. W. The Reaction of Hydrogen Atoms with Carbon Dioxide at 1200-1350°K. *J. Phys. Chem.* **1958**, 62, 1578-1581.

54. Vagner, P.; Kodym, R.; Bouzek, K. Thermodynamic Analysis of High Temperature Steam and Carbon Dioxide Systems in Solid Oxide Cells. *Sustainable Energy Fuels.* **2019**, 3, 2076-2086.

55. Fujita, J.; Hiyama, T.; Hirukawa, A.; Kondo, T.; Nakamura, J.; Ito, S.; Araki, R.; Ito, Y.; Takeguchi, M.; Pai, W. W. Near Room Temperature Chemical Vapor Deposition of Graphene with Diluted Methane and Molten Gallium Catalyst. *Sci. Rep.* **2016**, 7, 12371.

56. Zhang, C.; Lu, W.; Xie, X., Tang, D.; Liu, C.; Yang, Q. H. Towards Low Temperature Thermal Exfoliation of Graphite Oxide for Graphene Production. *Carbon* **2013**, 62, 11-24.

57. Chen, X.; Meng, D., Wang, B.; Li, B. W.; Li, W.; Bielawski, C. W.; Ruoff, R. S. Rapid Thermal Decomposition of Confined Graphene Oxide Films in Air. *Carbon* **2016**, 101, 71-76.

58. Rahman, O. S.A.; Mukherjee, B.; Islam, A.; Keshri, A. K. Instant Tuning of Superhydrophilic to Robust Superhydrophobic and Self-Cleaning Metallic Coating: Simple, Direct, One-Step, and Scalable Technique. *ACS Appl. Mater. Interfaces* **2019**, 11, 4616-4624.

59. Mukherjee, B.; Rahman, O. S. A.; Islam, A.; Pandey, K. K.; Keshri, A. K. Deposition of Multiscale Thickness Graphene Coating by Harnessing Extreme Heat and Rapid Quenching: Toward Commercialization. *ACS Appl. Mater. Interfaces* **2019**, 11, 25500-25507.

60. Ranjan, S.; Mukherjee, B.; Islam, A.; Pandey, K. K.; Gupta, R.; Keshri, A. K. Microstructure, Mechanical and High Temperature Tribological Behaviour of Graphene Nanoplatelets Reinforced Plasma Sprayed Titanium Nitride Coating. *J. Eur. Ceram.* **2020**, 40, 660-671.

61. Altman, I. S. On Principle Inadequacy of the Plank Distribution to The Spectrum of the Small Particle Thermal Radiation. *Physics Letters A* **1999**,256, 122-124.

62. Wang, W.; Wang, Y.; Gao, Y.; Zhao, Y. Control of Number of Graphene Layers Using Ultrasound in Supercritical CO_2 and Their Application in Lithium-Ion Batteries. *J. Supercrit. Fluids* **2014**, 85, 95-101.

63. Gadipelli, S.; Guo, Z. X. Graphene-Based Materials: Synthesis and Gas Sorption, Storage and Separation. *Prog. Mater. Sci.* **2015**, 69, 1-60.

64. Keshri, A. K.; Patel, R.; Agarwal, A. Comprehensive Process Maps to Synthesize High Density Plasma Sprayed Aluminum Oxide Composite Coatings with Varying Carbon Nanotube Content. *Surf. Coat. Technol.* **2010**, 205, 690-702.

65. Kim, J.; Kwon, S.; Cho, D-H.; Kang, B.; Kwon, H.; Kim, Y.; Park, S. O.; Jung, G. Y.; Shin, E.; Kim, W-G.; Lee, H.; Ryu, G. H.; Choi, M.; Kim, T. H.; Oh, J.; Park, S.; Kwak, S. K.; Yoon, S. W.; Byun, D.; Lee, Z.; *et al*. Direct Exfoliation and Dispersion of Two-Dimensional Materials in Pure Water *via* Temperature Control. *Nat Commun.* 2015, **6,** 8294.

66. Hadi, A.; Zahirifar, J.; Sabet, J. K.; Dastbaz, A. Graphene Nanosheets Preparation Using Magnetic Nanoparticle Assisted Liquid Phase Exfoliation of Graphite: The Coupled Effect of Ultrasound and Wedging Nanoparticles. *Ultrason Sonochem*. **2018**, 44, 204-214.

67. Hernandez, Y.; Nicolosi, V.; Lotya, M.; Blighe, F. M.; Sun, Z.; De, S.; McGovern, I. T.; Holland, B.; Byrne, M.; Gun'Ko, Y. K.; Boland, J. J.; Niraj, P.; Duesberg, G.; Krishnamurthy, S.; Goodhue, R.; Hutchison, J.; Scardaci, V.; Ferrari, A. C.; Coleman, J. N. High-Yield Production of Graphene by Liquid-Phase Exfoliation Of Graphite. *Nat. Nanotechnol.* **2008**,3, 563-568.

68. Voiry, D.; Yang, J.; Kupferberg, J.; Fullon, R.; Lee, C.; Jeong, H. Y.; Shin, H. S.; Chhowalla, M. High-Quality Graphene *via* Microwave Reduction of Solution-Exfoliated Graphene Oxide. *Science* **2016**,353, 1413-1416.

69. Li, X.; Cai, W.; An, J.; Kim, S.; Nah, J.; Yang, D.; Piner, R.; Velamakanni, A.; Jung, I.; Tutuc, E.; Banerjee, S. K.; Colombo, L.; Ruoff, R. S. Large-Area Synthesis of High-Quality and Uniform Graphene Films on Copper Foils. *Science* **2009**,324, 1312-1314.

70. Kovtyukhova, N. I.; Wang, Y.; Berkdemir, A.; Silva, R. C.; Terrones, M.; Crespi, V. H.; Mallouk, T. E. Non-Oxidative Intercalation and Exfoliation of Graphite by Brønsted Acids. *Nat. Chem.* **2014**, 6, 957-963.

71. Amiri, A.; Shanbedi, M.; Ahmadi, G.; Eshghi, H.; Kazi, S. N.; Chew, B. T.; Savari, M.; Zubir, M. N. M. Mass Production of Highly-Porous Graphene for High-Performance Supercapacitors. *Sci. Rep.* **2016**, 6, 32686.

72. Pfender, E.; Lee, Y. C. Particle Dynamics and Particle Heat and Mass Transfer in Thermal Plasmas . Part I . The Motion of a Single Particle without Thermal Effects, *Plasma Chem. and Plasma P.* **1985**, 5, 211-237.

73. Steward, E. G.; Cook, B. P.; Kellett, E. A. Dependence on Temperature of the Interlayer Spacing in Carbons of Different Graphitic Perfection, *Nature* **1960**, 187, 1015-1016.

74. Los, J. H.; Zakharchenko, K. V.; Katsnelson, M. I.; Fasolino, A. Melting Temperature of Graphene. *Phys. Rev. B - Condens. Matter Mater. Phys.* **2015**, 91, 1-6.

75. Ganz, E.; Ganz, A. B.; Yang, L. M.; Dornfeld, M. The Initial Stages of Melting of Graphene Between 4000 K and 6000 K. *Phys. Chem. Chem. Phys.* **2017**, 19, 3756-3762.

76. Russ, S.; Pfender, E.; Strykowski, P. J. Unsteadiness and Mixing in Thermal Plasma Jets. *Plasma Chem. and Plasma P.* **1994**, 14, 425-436.

77. Pfender, E. Plasma Jet Behaviour and Modelling Assisted with the Plasma Spray Process, *Thin Solid Films.***1994**, 238, 228-241.

78. Spores, R.; Pfender, E. Flow Structure of a Turbulent Thermal Plasma Jet. *Surf. Coat. Technol.* **1989**, 37, 251-270.

79. Fauchais, P.; Vardelle, A. Heat, Mass and Momentum Transfer in Coating Formation by Plasma Spraying. *Int. J. Therm. Sci.* **2000**, 39, 852-870.

80. Krejci, L.; Dolinek, V.; Ruzicka, B.; Chalupova, V.; Russ, S. Identification of the Laminar-Turbulent Transition Process in a Plasma Plume. *Plasma Chem. and Plasma P.* **1993**,601, 601-612.

81. Gupta, N.; Walia, S.; Mogera, U.; Kulkarni, G, U.; Twist-Dependent Raman and Electron Diffraction Correlations in Twisted Multilayer Graphene. *J. Phys. Chem. Lett.* **2020**, 11, 2797-2803.

82. Stanford, M. G.; Bets, K. V.; Luong, D. X.; Advincula, P. A.; Chen, W.; Li, J. T.; Wang, Z.; McHugh, E. A.; Algozeeb, W. A.; Yakobson, B. I.; Tour. J. M. Flash Graphene Morphologies. *ACS Nano* **2020**, 14, 13691–13699.

83. Bourlinos, A. B.; Georgakilas, V.; Zboril, R.; Steriotis, T. A.; Stubos, A. K.; Trapalis, C. Aqueous-Phase Exfoliation of Graphite in the Presence of Polyvinylpyrrolidone for the Production of Water Soluble Graphenes. Solid State Commun. **2009**, 149, 2172-2176

84. Loung, D. X.; Bets, K. V., Algozeeb, W. A.; Stanford, M. G., Kittrell, C.; Chen, W.; Salvatierra, R. V.; Ren, M.; McHugh, E. A.; Advincula, P. A.; Wang, Z.; Bhatt, M.; Guo, H.; Mancevski, V.; Shahsavari, R.; Yakobson, B. I.; Tour, J. M. Gram-Scale Bottom-Up Flash Graphene Synthesis. *Nature* **2020**, 577, 647-651.

85. Kwon, Y. J.; Kwon, Y.; Park, H. S.; Lee, J. U. Mass-Produced Electrochemically Exfoliated Graphene for Ultrahigh Thermally Conductive Paper Using a Multimetal Electrode System. *Adv. Mater. Interfaces*. **2019**, 6, 1900095.

86. Dominguez, J. M. G.; Leon, V.; Lucio, M. I.; Prato, M.; Vazquez, E. Production of Ready-to-Use Few-Layer Graphene in Aqueous Suspensions. *Nature Protocols*. **2018**, 13, 495-506.

87. Ejigu, A.; Fujisawa, K.; Spencer, B. F.; Wang, B.; Terrones, M.; Kinloch, I. A.; Dryfe, R. A. W. On the Role of Transition Metal Salts During Electrochemical Exfoliation of Graphite: Antioxidants or Metal Oxide Decorators for Energy Storage Applications. *Adv. Funct. Mater.* **2018**, 28, 1804357.

88. Buzaglo, M.; Bar, I. P.; Varenik, M.; Shunak, L.; Pevzner, S.; Regev, O. Graphite-to-Graphene: Total Conversion. *Adv. Mater.* **2017**, 29, 1603528.

89. Buzaglo, M.; Ruse, E.; Levy, I.; Nadiv, R.; Reuveni, G.; Shtein, M.; Regev, O. Top-Down, Scalable Graphene Sheets Production: It Is All about the Precipitate. *Chem. Mater.* **2017**, 29, 9998-10006.

90. Voiry, D.; Yang, J.; Kupferberg, J.; Fullon, R.; Lee, C.; Jeong, H. Y.; Shin, H. S.; Chhowalla, M. High-Quality Graphene *via* Microwave Reduction of Solution-Exfoliated Graphene Oxide. *Science* **2016**, 353, 1413-1416.

91. Yang, S.; Bruller, S.; Wu, Z. S.; Liu, Z.; Parvez, K.; Dong, R.; Richard, F.; Samori, P.; Feng, X.; Mullen, K. Organic Radical-Assisted Electrochemical Exfoliation for the Scalable Production of High-Quality Graphene. *J. Am. Chem. Soc.* **2015**, 137, 13927-13932.

92. Paton, K. R.; Varrla, E.; Backes, C.; Smith, R. J.; Khan, U.; O'Neill, A.; Boland, C.; Lotya, M.; Istrate, O. M.; King, P.; Higgins, T.; Barwich, S.; May, P.; Puczkarski, P., Ahmed, I.; Moebius, M.; Pettersson, H.; Long, E.; Coelho, J.; O'Brien, S. E. *et al*.

Scalable Production of Large Quantities of Defect-Free Few-Layer Graphene by Shear Exfoliation in Liquids. *Nat. Mater.* **2014**, 13, 624-630.

93. Matsumoto, M.; Saito, Y.; Park, C.; Fukushima, T.; Aida, T. Ultrahigh-Throughput Exfoliation of Graphite into Pristine 'Single-Layer' Graphene Using Microwaves and Molecularly Engineered Ionic Liquids. *Nat. Chem.* **2015**,**7**, 730-736.

94. Parvez, K.; Wu, Z. S.; Li, R.; Liu, X.; Graf, R.; Feng, X.; Mullen, K. Exfoliation of Graphite into Graphene in Aqueous Solutions of Inorganic Salts. *J. Am. Chem. Soc.* **2014**, 136, 6083-6091.

95. Du, W.; Jiang, X.; Zhu, L. From graphite to graphene: Direct Liquid-Phase Exfoliation of Graphite to Produce Single- and Few-Layered Pristine Graphene. *J. Mater. Chem. A* **2013**, 1, 10592–10606.

96. Leon, V.; Rodriguez, A. M.; Prieto, P.; Prato, M.;Vazquez, E. Exfoliation of Graphite With Trriazine Derivatives Under Ball-Milling Conditions: Preparation of Few-Layer Graphene *via* Selective Noncovalent Interactions. *ACS Nano.* **2014**, 8, 563-571.

97. Geng, X.; Guo, Y.; Li, D.; Li, W.; Zhu, C.; Wei, X.; Chen, M.; Gao, S.; Qiu, S.; Gong, Y.; Wu, L.; Long, M.; Sun, M.; Pan, G.; Liu, L. Interlayer Catalytic Exfoliation Realizing Scalable Production of Large-Size Pristine Few-Layer Graphene. *Sci. Rep.* **2013**, 3, 1134.

98. Yang, H.; Hernandez, Y.; Schlierf, A.; Felten, A.; Eckmann, A.; Johal, S.; Louette, P.; Pireaux, J. J.; Feng, X.; Mullen, K.; Palermo, V.; Casiraghi, C. A Simple Method for Graphene Production Based on Exfoliation of Graphite in Water Using 1-Pyrenesulfonic Acid Sodium Salt. *Carbon* **2013**, 53, 357-365.

99. You, S.; Luzan, S. M.; Szabo, T.; Talyzin, A. V. Effect of Synthesis Method on Solvation and Exfoliation of Graphite Oxide. *Carbon* **2013**, 52, 171-180.

100. Zhang, C.; Lu, W.; Xie, X.; Tang, D.; Liu, C.; Yang, Q. H. Towards Low Temperature Thermal Exfoliation of Graphite Oxide for Graphene Production. *Carbon* **2013**, 62, 11-24.

101. Liao, K.; Ding, W.; Zhao, B.; Li, Z.; Song, F.; Qin, Y.; Chen, T.; Wan, J.; Han, M.; Wang, G.; Zhou, J. High-Power Splitting of Expanded Graphite to Produce Few-Layer Graphene Sheets. *Carbon* **2011**, 49, 2862-2868.

102. Lu, W.; Liu, S.; Qin, X.; Wang, L.; Tian, J.; Luo, Y.; Asiri, A. M.; Youbi, A. O. A.; Sun, X. High-Yield, Large-Scale Production of Few-Layer Graphene Flakes within Seconds: Using Chlorosulfonic Acid and H_2O_2 as Exfoliating Agents. *J. Mater. Chem.* **2012**, 22, 8775-8777.

103. Herron, C. R.; Coleman, K. S.; Edwards, R. S., Mendis, B. G. Simple and Scalable Route for the 'Bottom-Up' Synthesis of Few-Layer Graphene Platelets and Thin Films. *J. Mater. Chem.* **2011**, 21, 3378-3383.

104. Ang, P. K.; Wang, S.; Bao, Q.; Thong, J. T. L.; Loh, K. P. High-Throughput Synthesis of Graphene by Intercalation-Exfoliation of Graphite Oxide and Study of Ionic Screening in Graphene Transistor. *ACS Nano.* **2009**, 3, 3587-3594.

105. Choi, E. Y.; Choi, W. S.; Lee, Y. B.; Noh, Y. Y. Production of Graphene by Exfoliation of Graphite in a Volatile Organic Solvent. *Nanotechnology* **2011**, 22, 365601.

106. Knieke, C.; Berger, A.; Voigt, M.; Taylor, R. N. K.; Rohrl, J.; Peukert, W. Scalable Production of Graphene Sheets by Mechanical Delamination. *Carbon* **2010**, 48, 3196-3204.

107. Zhu, Y.; Stoller, M. D.; Cai, W.; Velamakanni, A.; Piner, R. D.; Chen , D.; Ruoff, R. S. Exfoliation of Graphite Oxide in Propylene Carbonate and Thermal Reduction of the Resulting Graphene Oxide Platelets. ACS Nano **2010**, 4, 1227-1233.

108. Gu, W.; Zhang, W.; Li, X.; Zhu, H.; Wei, J.; Li, Z.; Shu, Q.; Wang, C.; Wang, K.; Shen, W.; Kang, F.; Wu, D. Graphene Sheets from Worm-Like Exfoliated Graphite. *J. Mater. Chem.* **2009**, 19, 3367-3369.

109. Hernandez, Y.; Nicolosi, V.; Lotya, M.; Blighe, F. M.; Sun, Z.; De, S.; McGovern, I. T.; Holland, B.; Byrne, M.; Gun'Ko, Y. K.; Boland, J. J.; Niraj, P.; Duesberg, G.; Krishnamurthy, S.; Goodhue, R.; Hutchison, J.; Scardaci, V.; Ferrari, A. C.; Coleman, J. N. High-Yield Production of Graphene by Liquid-Phase Exfoliation of Graphite. *Nat. Nanotechnol.* ***2008,***3, 563-568.

110. Stankovich, S.; Dikin, D. A.; Piner, R. D.; Kohlhaas, K. A.; Kleinhammes, A.; Jia, Y.;Wu, Y.; Nguyen, S. B. T.; Ruoff, R. S. Synthesis of Graphene-Based Nanosheets *via* Chemical Reduction of Exfoliated Graphite Oxide. *Carbon* **2007**, 45, 1558-1565.

111. Shang, N. G.; Papakonstantinou, P.; McMullan, M.; Chu, M.; Stamboulis, A.; Potenza, A.; Dhesi, S. S.; Marchetto, H. Catalyst-Free Efficient Growth, Orientation and Biosensing Properties of Multilayer Graphene Nanoflake Films with Sharp Edge Planes. *Adv. Funct. Mater.* **2008**, 18, 3506-3514.

112. Allen, M. J.; Wang, M.; Jannuzzi, S. A. V.; Yang, Y.; Wang, K. L.; Kaner, R. B. Chemically Induced Folding of Single and Bilayer Graphene. *Chem. Commun.* 2009, 6285-6287.

113. Papageorgiou, D. G.; Kinloch, I. A.; Young, R. J. Mechanical Properties of Graphene and Graphene-Based Nanocomposites. *Prog. Mater. Sci.* **2017**, 90,75-127.

114. Lipatov, A.; Lu, H.; Alhabeb, M.; Anasori, B.; Gruverman, A.; Gogotsi, Y.; Sinitskii, A. Elastic Properties of 2D $Ti_3C_2T_x$ MXene Monolayers and Bilayers. *Sci. Adv.* **2018**, 4, 1-7.

115. Lee, C.; Wei, X.; Kysar, J. W.; Hone, J. Measurement of the Elastic Properties and Intrinsic Strength of Monolayer Graphene. *Science* **2018**, 32, 385-388.

116. Suk, J. W.; Piner, R. D.; An, J.; Ruoff, R. S. Mechanical Properties of Monolayer Graphene Oxide. *ACS Nano* **2010**, 4, 6557-6564.

117. Cellini, F.; Lavini, F.; Berger, C.; Heer, W.; Riedo, E. Layer Dependence of Graphene-Diamene Phase Transition in Epitaxial and Exfoliated Few-Layer Graphene Using Machine Learning. *2D Mater*. **2019**, 6, 035043.

118. Polin, G.; Navarro, C. G.; Parente, V.; Guinea, F.; Katsnelson, M. I.; Murano, F. P.; Herrero, J. G. Increasing the Elastic Modulus of Graphene by Controlled Defect Creation. *Nature Phys.* **2015**, 11, 26-31.

119. Berman, D.; Erdemir, A.; Sumant,A. V. Graphene: A New Emerging Lubricant. *Matter. Today* **2014**, 17, 31-42.

120. Berman, D.; Erdemir, A.; Sumant, A. V. Few Layer Graphene to Reduce Wear and Friction on Sliding Steel Surfaces. *Carbon* **2013**, 54, 454-459.

121. Shin, Y. J.; Stromberg, R.; Nay, R.; Huang, H.; Wee, A. T. S.; Yang, H.; Bhatia, C. S. Frictional Characteristics of Exfoliated and Epitaxial Graphene. *Carbon* **2011**, 49, 4070-4073.

122. Zhao, W.; Fang, M.; Wu, F.; Wu, H.; Wang, L.; Chen, G. Preparation of Graphene by Exfoliation of Graphite Using Wet Ball Milling. *J. Mater. Chem.* **2010**, 20, 5817–5819.

123. Kalambate, P. K.; Dar, R. A.; Karna, S. P.; Srivastava, A. K. High Performance Supercapacitor Based on Graphene-Silver Nanoparticles-Polypyrrole Nanocomposite Coated on Glassy Carbon Electrode. *J. Power Source* **2015**, 276, 262-270.

124. Jia, B.; Zou, L. Graphene Nanosheets Reduced by a Multi-Step Process as High-Performance Electrode Material for Capacitive Deionisation. Carbon **2012**, 50, 2315-2321.

125. Quin, L.; L, Lu. Fabrication of Three-Dimensional Porous Graphene-Manganese Dioxide Composites as Electrode Material for Supercapacitors. *Colloids and Surfaces A: Pysiochem. Eng. Aspects* **2015**, 465, 32-38.

126. Chen, Y.; Zhang, X.; Yu, P.; Maa, Y. Electrophoretic Deposition of Graphene Nanosheets on Nickel Foams for Electrochemical Capacitors. *J. Power Source* **2010**, 195, 3031-3035.